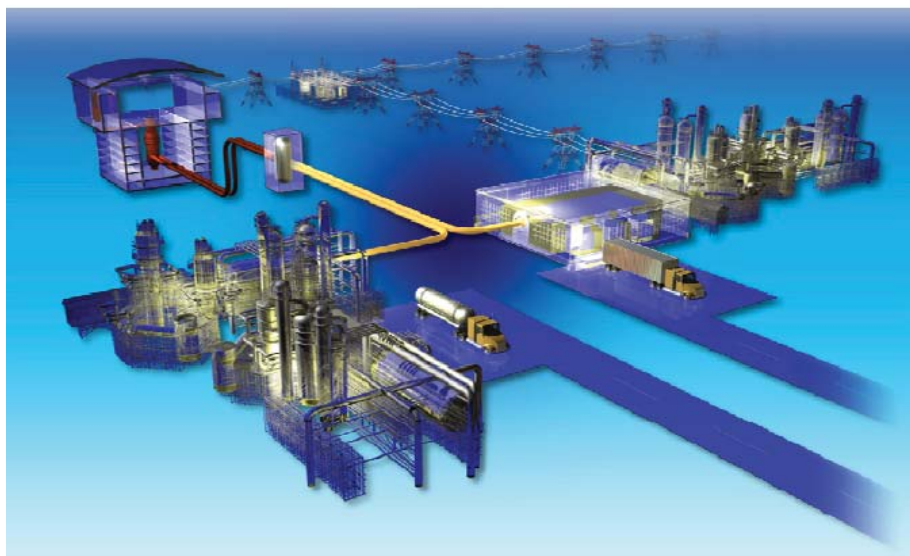


Hydrogen Permeability of Incoloy 800H, Inconel 617, and Haynes 230 Alloys

P. Calderoni
M. A. Ebner

July 2010



The INL is a U.S. Department of Energy National Laboratory
operated by Battelle Energy Alliance



DISCLAIMER

This information was prepared as an account of work sponsored by an agency of the U.S. Government. Neither the U.S. Government nor any agency thereof, nor any of their employees, makes any warranty, expressed or implied, or assumes any legal liability or responsibility for the accuracy, completeness, or usefulness, of any information, apparatus, product, or process disclosed, or represents that its use would not infringe privately owned rights. References herein to any specific commercial product, process, or service by trade name, trade mark, manufacturer, or otherwise, does not necessarily constitute or imply its endorsement, recommendation, or favoring by the U.S. Government or any agency thereof. The views and opinions of authors expressed herein do not necessarily state or reflect those of the U.S. Government or any agency thereof.

Hydrogen Permeability of Incoloy 800H, Inconel 617, and Haynes 230 Alloys

P. Calderoni and M. A. Ebner

July 2010

**Idaho National Laboratory
Next Generation Nuclear Plant Project
Idaho Falls, Idaho 83415**

**Prepared for the
U.S. Department of Energy
Office of Nuclear Energy
Under DOE Idaho Operations Office
Contract DE-AC07-05ID14517**

Next Generation Nuclear Plant Project

Hydrogen Permeability of Incoloy 800H, Inconel 617, and Haynes 230 Alloys

INL/EXT-10-19387

July 2010

Prepared by:



P. Calderoni

7-27-10

Date




M. A. Ebner

7-27-10

Date

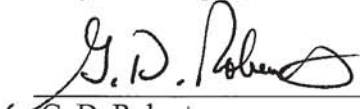
Approved by:



J. Simonds
Project Manager, AGR Fuel Development

7/28/10

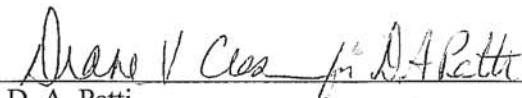
Date



G. D. Roberts
NGNP Quality Assurance Lead

7/27/2010

Date



D. A. Petti
Director, VHTR Technology Development Office

7/27/10

Date

ABSTRACT

A potential issue in the design of the Next Generation Nuclear Plant (NGNP) reactor and its high-temperature components is the permeation of fission generated tritium and hydrogen product from downstream hydrogen generation through high-temperature components. Such permeation can result in the loss of fission-generated tritium to the environment and the potential contamination of the helium coolant by permeation of product hydrogen into the coolant system. This issue will be addressed in the engineering design phase, and requires knowledge of permeation characteristics of the candidate alloys. Of the three potential candidates for high-temperature components of the NGNP reactor design, only hydrogen permeability for Incoloy 800H has been well documented, but at relatively high partial pressures of hydrogen. Hydrogen permeability data have been published for Inconel 617, but only in two literature reports and for partial pressures of hydrogen greater than one atmosphere, far higher than anticipated in the NGNP reactor. The hydrogen permeability of Haynes 230 has not been published.

To support engineering design of the NGNP reactor components, the hydrogen permeability of Inconel 617 and Haynes 230 were determined using a measurement system designed and fabricated at Idaho National Laboratory. The performance of the system was validated using Incoloy 800H as reference material, for which the permeability has been published in several journal articles. The permeability of Incoloy 800H, Inconel 617, and Haynes 230 was measured in the temperature range 650 to 950°C and at hydrogen partial pressures of 10^{-3} and 10^{-2} atm—substantially lower pressures than used in the published reports. The measured hydrogen permeability of Incoloy 800H and Inconel 617 were in good agreement with published values obtained at higher partial pressures of hydrogen. The hydrogen permeability of Inconel 617 and Haynes 230 were similar, about 50% greater than for Incoloy 800H and with similar temperature dependence.

CONTENTS

ABSTRACT.....	v
1. INTRODUCTION.....	1
2. OBJECTIVES OF THE RESEARCH.....	5
3. DESCRIPTION OF THE MEASUREMENT SYSTEM, SAMPLES, AND TEST PARAMETERS.....	6
3.1 Permeation Measurement System.....	6
3.2 Test Samples.....	14
3.3 Gas Mixtures.....	18
3.4 Test Parameters.....	18
3.5 Reference Materials.....	18
4. MEASUREMENT RESULTS.....	20
5. CONCLUSIONS.....	26
6. REFERENCES.....	28
Appendix A—Summary of Incoloy 800H Permeability Data.....	30
Appendix B—Summary of Inconel 617 Permeability Data.....	34
Appendix C—Summary of Haynes 230 Permeability Data.....	38

FIGURES

Figure 1. Hydrogen permeability of some metals, classes of alloys, and ceramics as a function of temperature. ¹	2
Figure 2. Summary of literature data for hydrogen permeability through Incoloy 800/800H.	3
Figure 3a. Schematic diagram of the primary loop of the permeability measurement system.	7
Figure 3b. Schematic diagram of the secondary loop of the permeability measurement system.	8
Figure 4. The permeability measurement system assembled within a glove box for eventual work with tritium permeation.....	9
Figure 5. Configuration of the test sample. The picture and drawing show the configuration of the test sample within the quartz-walled test chamber, surrounded by the induction heater coils.....	11
Figure 6. Sample output of the thermal imaging system.	13
Figure 7. Configuration of the test sample.....	15

Figure 8. Microstructure of the cross section of as-received Incoloy 800H tube stock.	16
Figure 9. Microstructure of the cross section of as-received Inconel 617 tube stock.	17
Figure 10. Microstructure of the cross section of as-received Haynes 230 tube stock.	17
Figure 11. Example of hydrogen flux through a sample in a test, as measured by the rise in hydrogen concentration in the sweep gas flow of the secondary loop.	20
Figure 12. Hydrogen permeability of Incoloy 800H from this work compared with published data, and show the uncertainty limits of the data.	24
Figure 13. Hydrogen permeability of Inconel 617 compared with the Incoloy 800H data from this work and the two sets of published data.....	25
Figure 14. Hydrogen permeability of Haynes 230 compared with the Incoloy 800H data from this work.	26

TABLES

Table 1. Literature values of the permeability constant and activation energy for hydrogen permeation through Incoloy 800/800H, Inconel 617, and Haynes 230	4
Table 2. Sources of Components.....	10
Table 3. Composition of the Incoloy 800H, Inconel 617, and Haynes 230 used in permeation tests.....	14
Table 4. Measured wall thickness of the as-received alloy tube stock.	14
Table 5. Measured hydrogen permeability values of Incoloy 800H, Inconel 617, and Haynes 230.	22
Table 6. Comparison of measured hydrogen permeability of Incoloy 800H with literature values for Incoloy 800/800H.	23
Table A-1. Test parameters and hydrogen permeation flow data for Incoloy 800H.....	31
Table A-2. Hydrogen permeability coefficients for Incoloy 800H.	32
Table B-1. Test parameters and hydrogen permeation flow data for Inconel 617.....	35
Table B-2. Hydrogen permeability coefficients for Inconel 617.	36
Table C-1. Test parameters and hydrogen permeation flow data for Haynes 230.....	39
Table C-2. Permeability coefficients for Haynes 230.	40

Hydrogen Permeability of Incoloy 800H, Inconel 617, and Haynes 230 Alloys

1. INTRODUCTION

The U.S. Department of Energy has selected the very high temperature reactor (VHTR) concept for the Next Generation Nuclear Plant (NGNP). Conceptually, the NGNP can produce electricity, generate hydrogen, and provide industrial process heat at temperatures up to 850°C. The NGNP design is conceptually a graphite reactor core in which the primary coolant is re-circulating helium gas. The very high outlet temperatures impose severe service requirements on the structural components of the reactor and intermediate heat exchanger. The need for resistance to high temperature creep severely limits candidate alloys to high-nickel alloys. Presently, alloys that are candidates for high-temperature structural components are Incoloy 800H, Inconel 617, and Haynes 230.¹

Containment of fission products is a paramount concern in the operation of a nuclear reactor. The containment of tritium, a gaseous fission product, is of special concern in the NGNP because of its high relative mobility in the core at the high operating temperatures. Tritium will be produced in the NGNP reactor as a tertiary fission product and by activation of: 1) graphite core contaminants such as lithium (Li-6 and Li-7); 2) the helium isotope, He-3, which is naturally present in the helium gas coolant; and 3) the boron in the B₄C burnable poison. Tritium is a radioactive isotope of hydrogen. It is an internal radiological hazard to humans, whose release is stringently limited by federal regulations. Because of its potentially high mobility at the reactor outlet temperatures, tritium poses a risk of permeating through the walls of the intermediate heat exchanger and steam generator systems, potentially contaminating the environment and the hydrogen product. Therefore, the stringent environmental regulatory limits require that the design of the core and the plant system effectively contain the tritium produced by fission and activation.

The design of an acceptable containment system requires the selection of materials that allow the control of fission product permeation. This is particularly important for the alloys comprising the high-temperature service components of the NGNP system such as the intermediate heat exchanger and the steam generator. Most gases, including hydrogen and tritium, have a finite permeation rate through materials, which generally increases exponentially with temperature. The magnitude of the permeation rate at any temperature is a function of the activation energy and the permeation constant (the Arrhenius frequency factor or pre-exponential factor), which are characteristics determined by the elemental composition, phase composition, microstructure, and surface coatings of the alloys and materials. The characterization of the permeation process is therefore essential for the design of control systems to ensure that emission limits are satisfied under all credible circumstances.

The permeation of hydrogen through the more common metals and alloys has been investigated extensively over the last 50 years. Permeation data have been published for a number of metal alloys, including ferritic steels, austenitic steels, copper alloys, aluminum alloys, some high-nickel alloys, and metals such as nickel, gold, and palladium for temperatures up to 600–900°C, as shown in Figure 1.¹ In general, the hydrogen permeability in metals is an exponential function of temperature, increasing as much as five orders of magnitude between 20 and 800°C. In addition, while the range of permeability for various groups of alloys spans many orders of magnitude at 20°C, the range decreases to a spread of only a few orders of magnitude at high temperatures (>500°C).

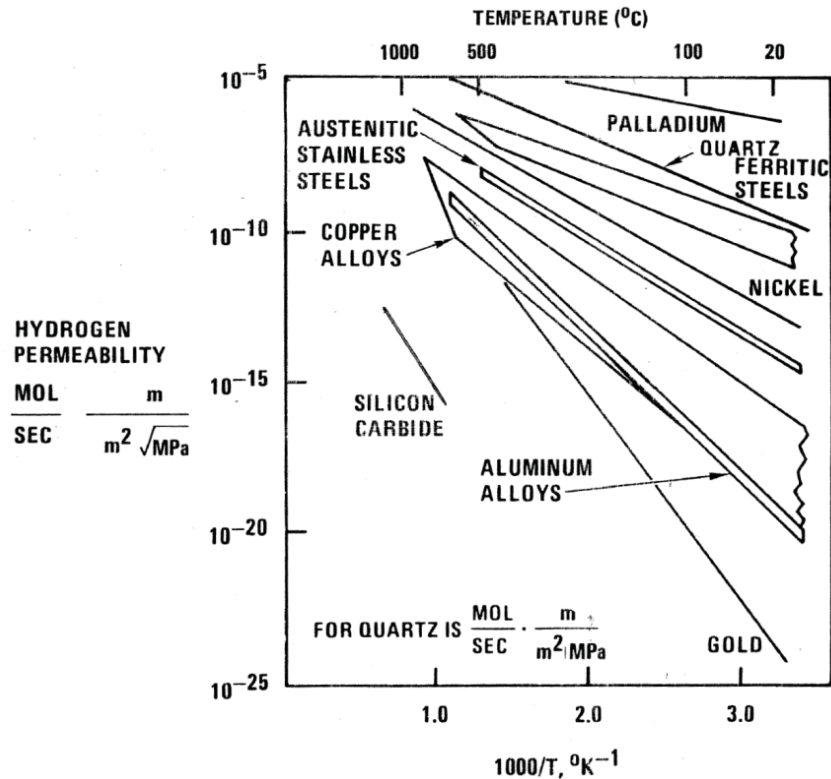


Figure 1. Hydrogen permeability of some metals, classes of alloys, and ceramics as a function of temperature.¹

The hydrogen permeability of the candidate alloys for NGNP structural components is not as well defined. Of the three candidate high-nickel alloys, only Incoloy 800/800H has been significantly tested for permeation, with several reports in the literature.^{2,3,4,5,6,7,8,9,10} By comparison, only two groups have reported hydrogen permeability data for Inconel 617 and none for Haynes 230.^{5,7} (Of the three alloys, tritium permeation has been reported only for Incoloy 800/800H, and only by two groups.^{5,12,13}) The accessible literature data for the permeation of hydrogen through Incoloy 800/800H are shown graphically in Arrhenius format in Figure 2. The activation energy for hydrogen permeation, Q (in units of kcal/mol), and the permeability constant, K_0 (in units of cm^3 [standard temperature and pressure (STP; 0°C, 1 atmosphere)] hydrogen/cm·sec·atm^{1/2}) are given in Table 1 for Incoloy 800/800H and Inconel 617, along with the applicable temperature and pressure ranges for the literature data. No permeability data for Haynes 230 have been found. As indicated in Table 1, the literature data generally pertain to hydrogen partial pressures greater than 0.1 atm, with the exception of the data of Roehrig et al.,⁴ and all are substantially higher than hydrogen and tritium pressures typical of the steady-state conditions within a VHTR core, at which a different permeation mechanism may operate. These data must be generated experimentally to support the design of the NGNP systems.

Because high temperature permeation measurement systems are not available commercially, a system suitable for the task was designed and built as part of the permeation measurement task.

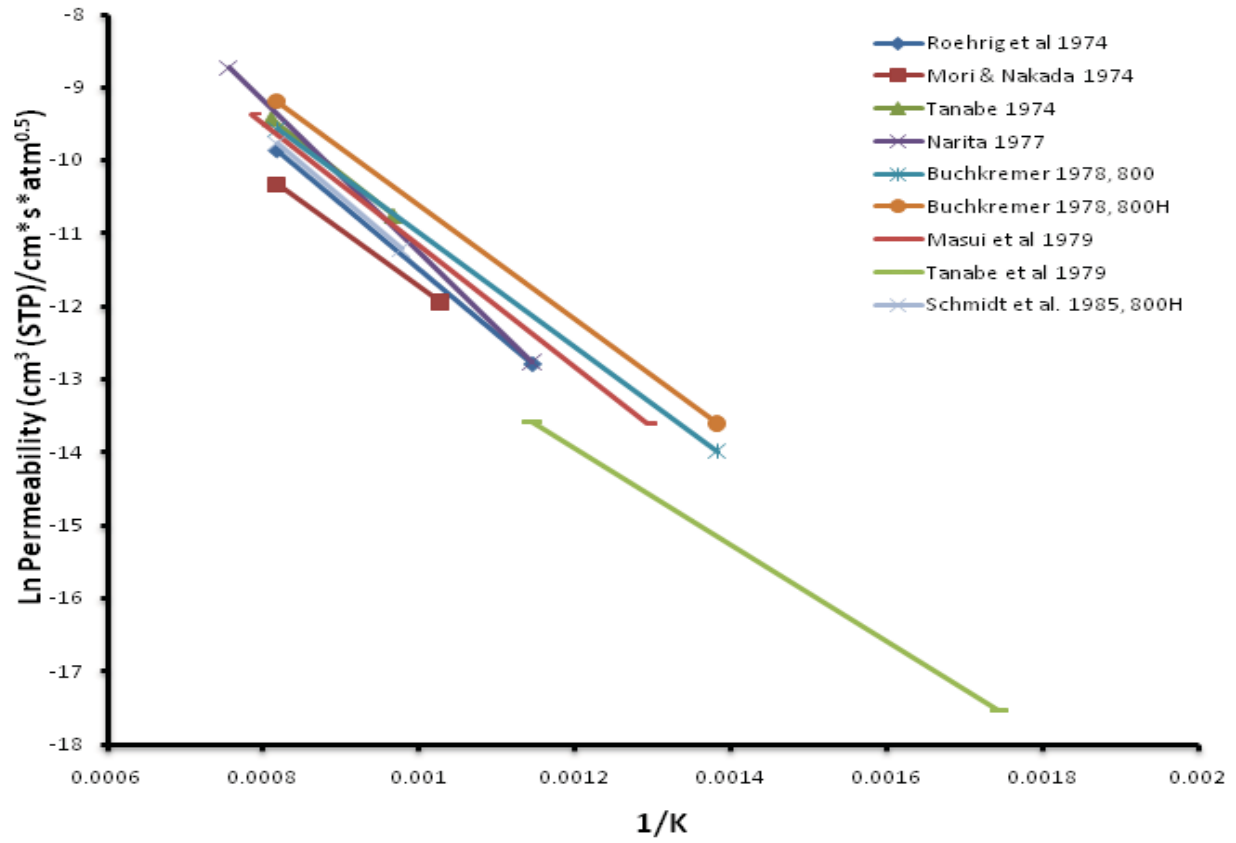


Figure 2. Summary of literature data for hydrogen permeability through Incoloy 800/800H.

Table 1. Literature values of the permeability constant and activation energy for hydrogen permeation through Incoloy 800/800H, Inconel 617, and Haynes 230

K_0 $\text{cm}^3 \text{H}_2 (\text{STP})/\text{cm}\cdot\text{sec}\cdot\text{atm}^{1/2}$	Q kcal/mol	Temp. Range $^{\circ}\text{C}$	Pressure Range atm	References
Incoloy 800, Hydrogen Permeability				
7.39×10^{-2}	17.7	600–950	$5 \times 10^{-4} - 0.5$	4
1.76×10^{-2}	15.3	700–950	1–5	2
7.58×10^{-2}	16.8	760–960	1	8
4.03×10^{-1}	20.6	600–1050	1–10	7
4.02×10^{-2}	15.5	450–950	5–10	9,11
$5.90 \times 10^{-2} *$	15.5 *	450–950	5–10	9,11
6.02×10^{-2}	16.6	500–1000	0.1–1	3
2.44×10^{-3}	13.1	300–600	0.13–0.8	6
$9.24 \times 10^{-2} *$	18.0 *	750–950	<40	5
Incoloy 800, Tritium Permeability				
2.60×10^{-2}	16.1	350–750	2 ppm ^3H , 1 atm H_2	12, 13
1.50×10^{-3}	13.5	750–950	1×10^{-4}	5
Inconel 617, Hydrogen Permeability				
2.28×10^{-1}	18.9	600–1050	1–10	7
1.39×10^{-1}	19.8	750–950	<40	5
Haynes 230, Hydrogen Permeability				
No reports	No reports			
* Data for Incoloy 800H				

2. OBJECTIVES OF THE RESEARCH

The objective of the Fission Product Transport-Tritium Permeation work is to experimentally determine the permeation rates of tritium through the candidate alloys for NGNP structural components, which include Incoloy 800H, Inconel 617, and Haynes 230. The work consists of three phases: (1) Design, fabrication, testing, and validation of the performance of a system for measuring permeation, using reference material; (2) Determination of the permeability of hydrogen through the three candidate alloys at low partial pressures of hydrogen; and (3) Determination of tritium permeation through the same alloys. The permeability measurement system is a custom design fabricated at Idaho National Laboratory. It was designed for operation with hydrogen or tritium, either as a single-pass or as a recirculation system, and operating at temperatures in the range 650 to 950°C at hydrogen pressures as low as 10^{-3} atm. The performance of the system was verified by measuring the hydrogen permeability of Incoloy 800H. The hydrogen permeability of Haynes 230 and Inconel 617 was measured in the range 650 to 950°C at hydrogen partial pressures of 10^{-3} and 10^{-2} atm.

This report summarizes the fabrication and performance testing of a custom system for measuring hydrogen permeability at high temperatures, and the measurement of hydrogen permeability through the candidate alloys.

3. DESCRIPTION OF THE MEASUREMENT SYSTEM, SAMPLES, AND TEST PARAMETERS

3.1 Permeation Measurement System

The measurement of hydrogen permeation through alloys at high temperatures imposes significant requirements on a measurement system. For accurate measurement of permeation at high temperatures, such a system must be able to:

- Accurately maintain a constant concentration of hydrogen over the sample.
- Accommodate interchangeable samples of metal alloys.
- Reach and maintain sample temperatures in the range of 650 to 950°C.
- Control the heated sample area for accuracy in permeation measurement.
- Minimize thermal inertia during heating and thermal cycling, for rapid sample temperature response.
- Allow fast and repeated temperature cycles (less than an hour per cycle) through temperature differentials of several hundred degrees Celsius.
- Accurately control the flow rate and pressure of the gases in the primary and secondary gas loops, and achieve flow rates in the range of 0.5 to 10 L/min.
- Accurately control and measure the permeating gas concentration (hydrogen and tritium) in the primary and secondary loops. Detection limits for hydrogen in the secondary loop must be 10 ppm or better, and for tritium in the 1 to 1,000 $\mu\text{Ci}/\text{m}^3$ range (corresponding to 1.5 to 1,500 ppm at STP).
- Accurately measure and control the concentration of oxidants in the primary and secondary loops in the 0.1 to 1,000 ppm range at STP.
- Operate the primary and secondary loops in a single-pass flow-through mode, and for increased sensitivity for tritium permeation test, in a re-circulation mode.

Such high-temperature permeation measurement systems are not available commercially as turn-key systems, but must be designed and built to suit the specific requirements of the task. Therefore, the NGNP project designed and assembled a system for the measurement of the permeation characteristics of hydrogen and tritium through metal samples at high temperatures.

The measurement system, shown by the simplified diagrams of Figure 3a and 3b, consists of two counter-flowing helium gas flow loops separated by the heated tubular test sample. The thin-walled tubular sample, mounted within a sealed quartz sample chamber, is the permeation interface separating the counter-flowing helium gas streams of the primary and secondary gas loops. The probe gas mixture (helium and hydrogen) in the primary gas loop flows through the bore of the tubular test sample, while the helium of the secondary gas loop, which includes the volume of the test chamber, flows over the external surface of the tubular sample to sweep away the permeated gas. The concentration of the permeated gas in the helium of the secondary gas loop is measured by a quadrupole mass spectrometer and, in planned tritium measurements, by a tritium detector.

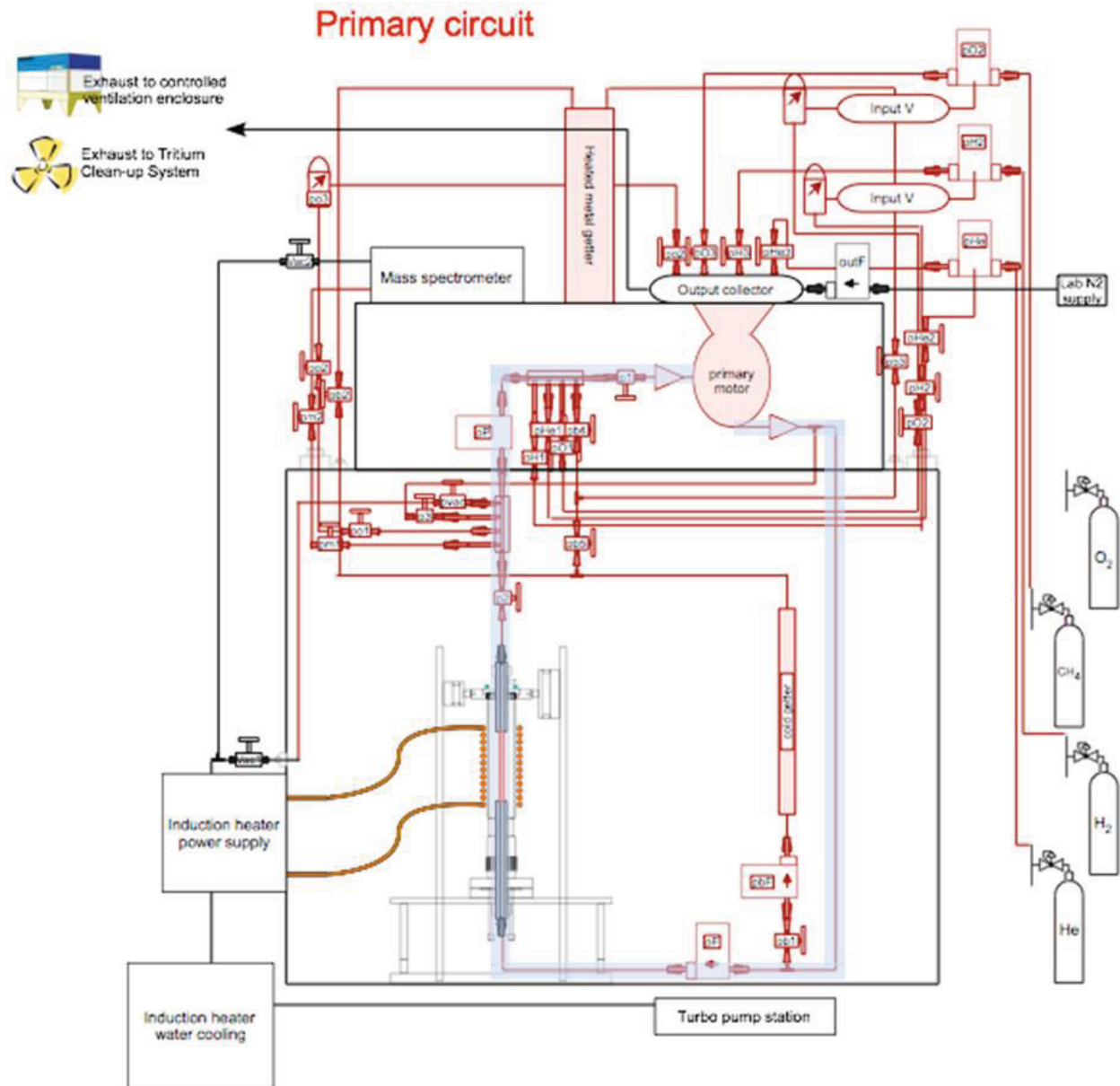


Figure 3a. Schematic diagram of the primary loop of the permeability measurement system.

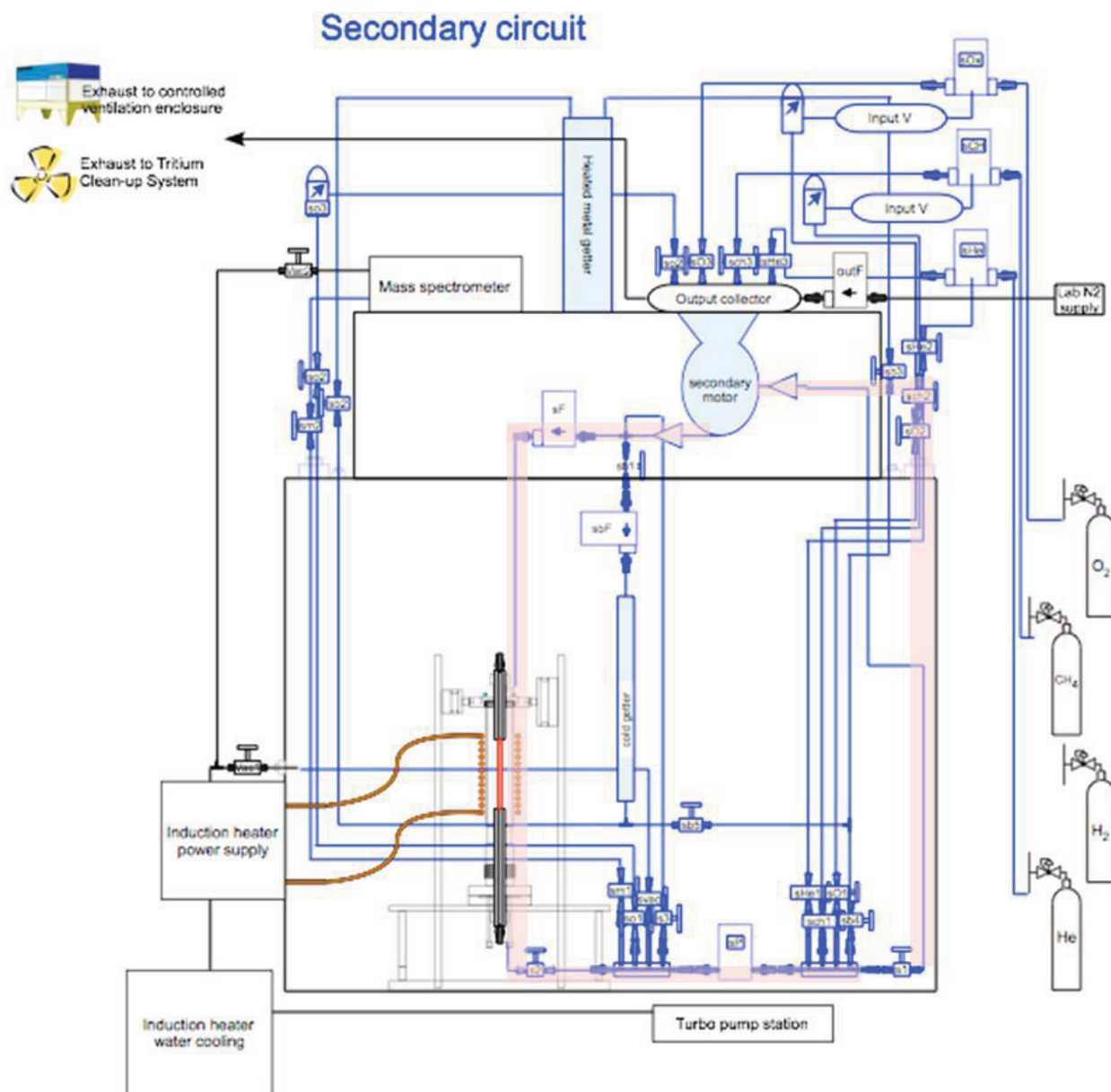


Figure 3b. Schematic diagram of the secondary loop of the permeability measurement system.

The permeation measurement system is a sealed system housed in a glove box, as shown in Figure 4, for tritium control in planned tritium testing. The system was fabricated with 316 and 304 stainless steel components, tubing, and welded compression fittings for vacuum integrity. Component sources for the measurement system are listed in Table 2. During the assembly and initial performance testing, the vacuum integrity of the system was established at a leak rate of less than 10^{-5} atm-cc/sec by helium leak testing with mass spectrometry. The system has provisions for introduction of certified hydrogen-helium gas mixtures used for the permeation probe mixture in the primary loop, introduction of ultra-high purity helium for the sweep gas in the secondary loop, getter modules for purification of the helium gas streams, a rotary pump and turbomolecular vacuum pump for evacuation and clean up of the gas loops, and metal bellows pumps for the circulation of the gas flows in the loops.

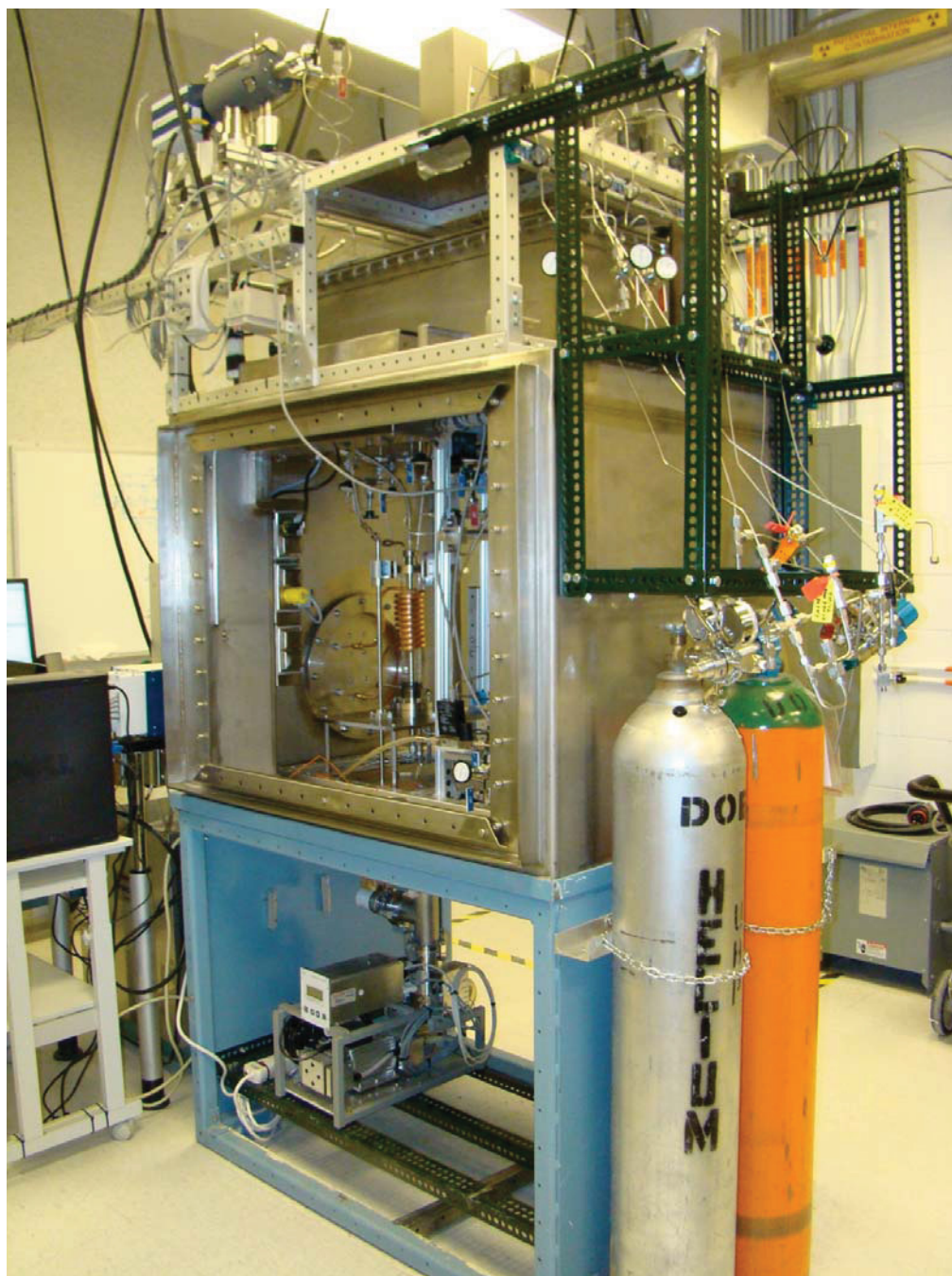


Figure 4. The permeability measurement system assembled within a glove box for eventual work with tritium permeation.

Table 2. Sources of Components.

Component	Item	Model	Manufacturer
Compression fittings	—	VCR	Swagelok, Inc.
Purification getters	—	HP-2, P100-2	VICI Valco Instruments Company, Inc
Rotary pump	—	RV5	Edwards, Inc.
Turbomolecular pump	—	TMH 071P	Pfeiffer Vacuum, Inc.
Metal bellows pumps	—	MB-158	Senior Operations, Inc.
Pressure controller	Transducer	PCD-30PSIA-D-25VCRM/5P	Alicat Scientific, Inc.
	Software	Flow Vision™ SC	Alicat Scientific, Inc.
Mass flow controllers	Transducer	MC-10SLPM-D-30PSIA-25VCRM	Alicat Scientific, Inc.
	Software	Flow Vision™ SC	Alicat Scientific, Inc.
	Transducer	C-100L-DD-8-OV1-PV2-V1-SI-CN	Sierra Instruments, Inc.
	Software	Smart-Trak 2™	Sierra Instruments, Inc.
Process control software	—	LabVIEW, version 8.5.1	National Instruments, Inc.
Mass spectrometer	Spectrometer	Transpector CPM Compact Process Monitor	Inficon, Inc.
	Software	TWare32™	Inficon, Inc.
Sample chamber	—	—	Larsen Glass, Inc.
Induction heater	—	SI-10KWHF	Superior Induction Co.
Control thermocouple	Type K thermocouple	—	Omega, Inc.
	Read out unit	SXCI-1000	National Instruments, Inc.
Thermal imaging system	Infrared camera	M9200	Mikron Infrared, Inc.
	Software	MikroSpec R/T™ 9200, Version 3.9200.117,	Mikron Infrared, Inc.
Alloys for samples	Incoloy 800H, Inconel 617, and Haynes 230	—	Century Tubes, Inc.
Sample supports	Inconel 600 tubes	—	TW Metals, Inc.
Gas mixtures	100, 1,000, and 10,000 ppm H ₂ in He	—	Norco, Inc.

The system is instrumented with pressure and mass flow controllers for accurate control of the helium pressure and flow rate. The operation of the pressure and mass flow controllers is controlled by Flow Vision™ SC software by Alicat, and the Sierra controllers by Smart-Trak 2™ software. Both software packages are interfaced with the LabVIEW process control software system used to manage the testing process. The composition of the input gas mixtures (100, 1,000, and 10,000 ppm hydrogen in helium) in the primary loop and the output gas in the secondary loop were measured by an in-line quadrupole mass spectrometer, which is capable of sampling gas streams at 1 atm pressure. The operation of the mass spectrometer and data acquisition from the mass spectrometer is controlled by Inficon TWare32™ software.

The sample chamber consists of a quartz tube sealed to Kovar transitions between two vacuum flanges, as shown diagrammatically in Figures 3 (above) and 5. The vacuum flanges are fitted with inlet and outlet Swagelock fittings for the secondary gas loop. The test sample is mounted in the upper and lower vacuum flange by compression O-ring seals, and is terminated with VCR gas compression fittings for connection to the primary loop. In this design, the two helium loops sweep the sample chamber in counter-flow manner, with the hydrogen-helium probe gas mixture passing upwards through the bore of the tubular sample, and the helium sweep flow of the secondary loop sweeping the external surface of the tubular sample, flowing downwards through the main chamber volume.

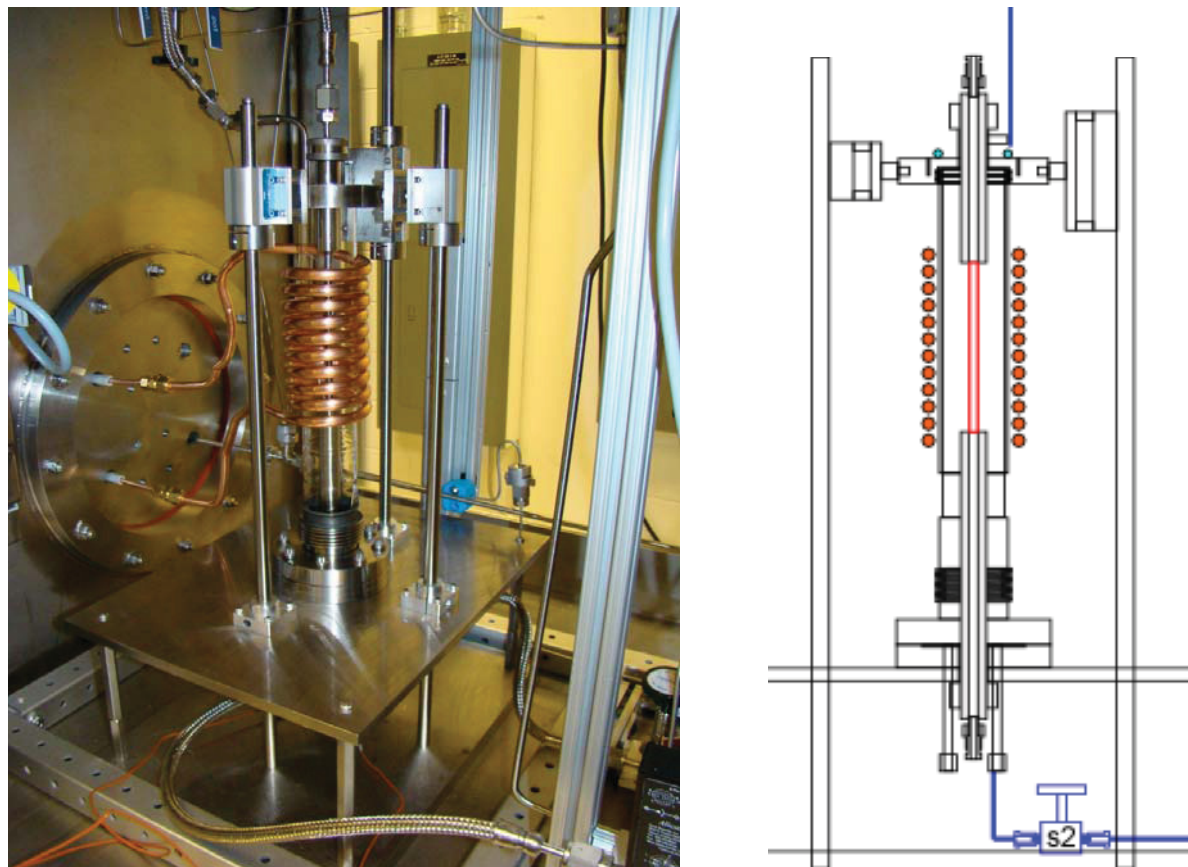
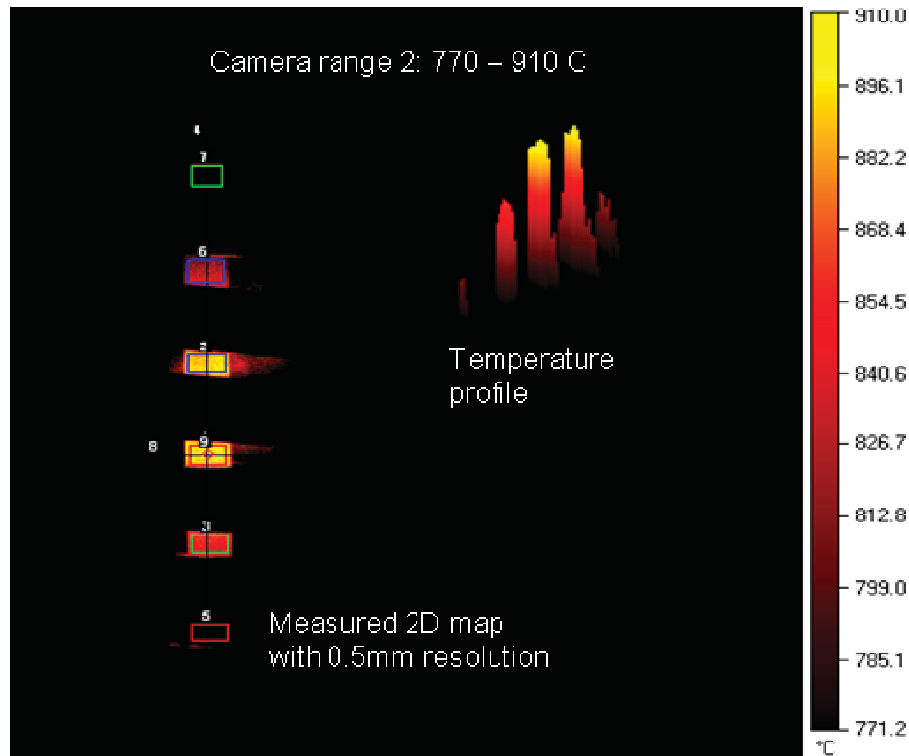


Figure 5. Configuration of the test sample. The picture and drawing show the configuration of the test sample within the quartz-walled test chamber, surrounded by the induction heater coils.

The test sample is directly heated by a radio frequency induction heater, with the copper coils external to the quartz chamber and surrounding the thin-walled section of the test sample, as shown in Figure 5. The induction heater heats the sample to temperature rapidly, within a few tenths of a second, defining a sharp temperature transition and avoiding the long temperature ramps that are common with resistance heaters. The induction heater is a water-cooled 440 Vac, 100 to 300 kHz, 10 kW system. The power output of the induction heater is controlled by the process control software interface LabVIEW, coupled with a thermocouple data acquisition unit from National Instruments, Inc. The control signal is acquired by a control thermocouple that is located inside the tubular test sample (manual control by the operator is also possible). The control thermocouple junction is located at the center (midplane) of the heated area of the test sample, in contact with the inner surface of the sample wall.

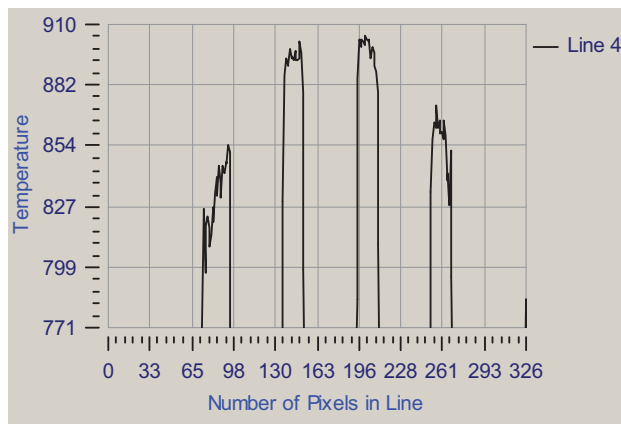
The temperature of the heated area of the test sample is monitored by an infrared thermal imaging system mounted externally to the quartz tube and the glove box. The system yields two-dimensional maps

of the temperatures of the heated sample area that is visible in the gaps between the induction heater coils. The system software provides four user-selectable temperatures ranges that span 600 to 1600°C for optimum sensitivity, with spectral response in the range of 800 to 900 nm (nanometers) and temperature resolution 0.5% of reading. The system permits the user to select up to 32 regions of interest in the image, and reports the minimum, maximum, and average temperatures of areas selected by the user, with spatial resolution of 0.5 mm, for an accurate assessment of the heated area and the temperature distribution in the heated area. The thermal imaging system is calibrated against the control thermocouple positioned within the sample, and thereby permits the evaluation of the emissivity and of the surface condition of the heated portion of the sample. A sample of the output is given in Figure 6, which images the areas of the heated Incoloy 800H sample that are visible between the windings of the induction coil. Figure 6 shows six areas of interest (oblong boxes) that correspond to the heated 800H sample visible between the induction coil windings, along with the corresponding graphical temperature profile, a tabulation of minimum, maximum, and average temperatures for each region of interest, and vertical (axial) and horizontal temperature profiles of the heated sample.



	Min. °C	Max. °C	Avg. °C	Range °C
Rectangle 1	880.9	908.8	895.5	27.9
Rectangle 2	876.3	905.0	891.5	28.7
Rectangle 3	828.3	871.5	852.1	43.2
Line 4	UNDER	902.0	UNDER	
Rectangle 5	UNDER	759.0	714.1	
Rectangle 6	787.4	852.8	824.0	65.4
Rectangle 7	UNDER	719.1	UNDER	
Line 8	UNDER	903.9	803.6	
Circle 9	888.4	902.9	895.7	14.5

Axial temperature profile through heated zone (vertical line in thermal image).



Horizontal temperature profile at center of heated zone (horizontal line in thermal image)

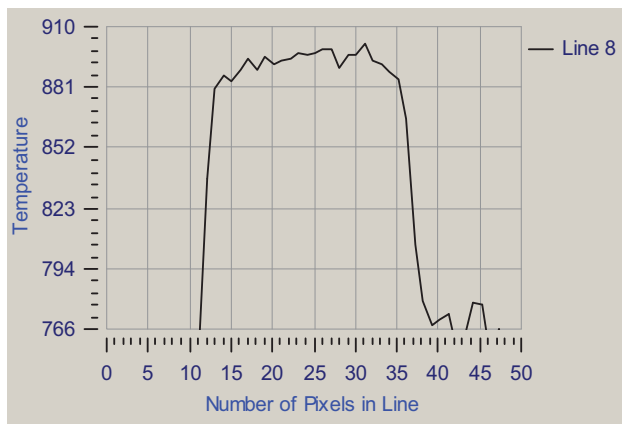


Figure 6. Sample output of the thermal imaging system.

3.2 Test Samples

The three alloys tested for hydrogen permeability are Incoloy 800H, Inconel 617, and Haynes 230. The composition of the alloy heats is given in Table 3. These alloys were obtained as thin-walled tubing stock from Century Tubes, Inc., and were used without further preparation other than the machining and cleaning required for welding into the sample configuration.

Table 3. Composition of the Incoloy 800H, Inconel 617, and Haynes 230 used in permeation tests.

Composition	Heat No.	Fe	Ni	Cr	Co	Mo	W	C	Al	
Incoloy 800H, 0.01, 0.03 in. wall	V01283	46.65	30.84	19.76				0.06	0.37	Ti: 0.48; Si:0.49; Mn: 1.14; Cu: 0.07
Inconel 617, 0.01 and 0.03 in. wall	XX58A7UK	1.55	53.02	22.21	12.46	8.97		0.08	1.04	Ti: 0.29; Si:0.17; Mn: 0.07; Cu: 0.14
Haynes 230 0.01 in. wall	8305-5-7171	0.94	59.48	22.39	0.19	1.36	14.26	0.11	0.37	Mn: 0.50; Si:0.38; La:0.015
Haynes 230 0.03 in. wall	8305-8-7372	1.44	59.41	21.63	0.75	1.12	14.28	0.09	0.35	Mn: 0.49; Si:0.42; La:0.009

The alloy tube stock was obtained in two wall thicknesses, nominally 0.010 and 0.030 in. (0.254 and 0.762 mm). The diameter of the tube stock is 0.25 in. (6.35 mm). The actual wall thickness of the alloy tube stock was determined by scanning electron microscopy (SEM) of radially sectioned and polished samples. The measurements were acquired at 100× magnification in backscattered electron imaging mode for optimum contrast, with the electronic dimensioning feature of the SEM (Model XL 30 ESEM, Philips Electron Optics, Inc.). The measurement uncertainty of electronic dimensioning feature is 3% of reading. The measured wall thickness for the samples, including total measurement uncertainty (because of electronic measurement uncertainty and the standard deviation in reading selections), is summarized in Table 4.

Table 4. Measured wall thickness of the as-received alloy tube stock.

Alloy	Wall Thickness (mm)		
	Nominal	Measured	Total Uncertainty(%)
Incoloy 800H	0.254	0.260	4.75
	0.762	0.798	3.61
Inconel 617	0.254	0.257	4.46
	0.762	0.785	3.66
Haynes 230	0.254	0.269	3.32
	0.762	0.781	3.40

The sample configuration is shown in Figure 7, and consists of a 4 to 6-in.-long test section of Incoloy 800H, Inconel 617, or Haynes 230 tube welded to upper and lower thick-walled barrels of Inconel 600. The Inconel 600 tubes are 0.75 in. (19.1 mm) outer diameter and 0.25 in. (6.35 mm) inner diameter; the tubes were gun-drilled from round bar stock. The center portion of the thin-walled test section is the heated permeation zone. The thickness of the barrels and their location outside the heated zone ensure that they do not contribute measurably to the flux of permeating gas. The thick-walled barrel sections of the test sample are sealed by compression O-ring seals to the upper and lower mounting flange of the sample chamber, thereby isolating the primary flow loop from the secondary flow loop.

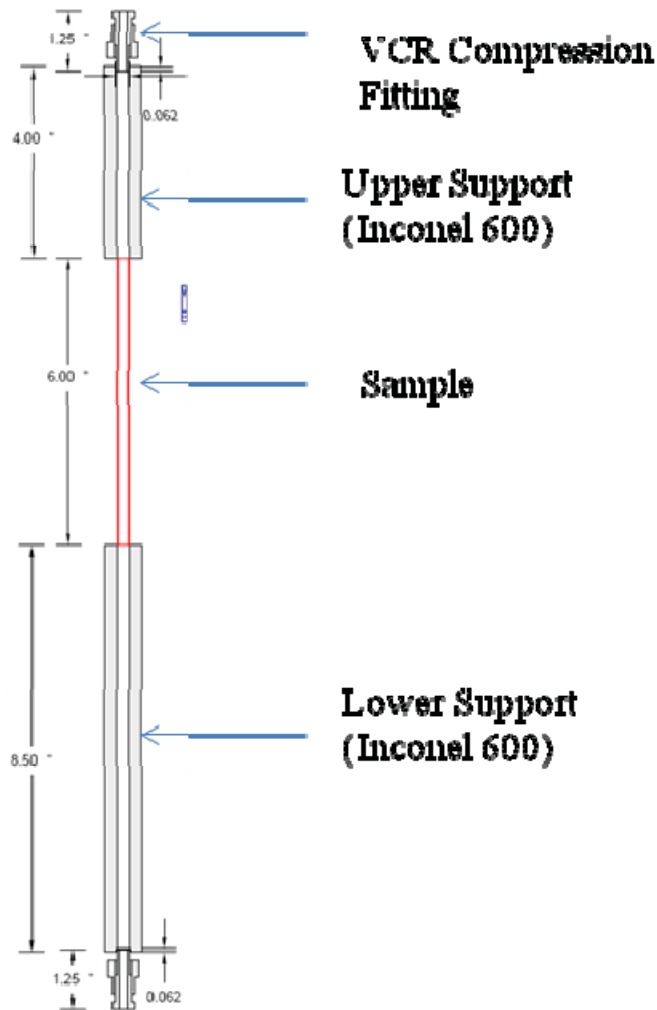
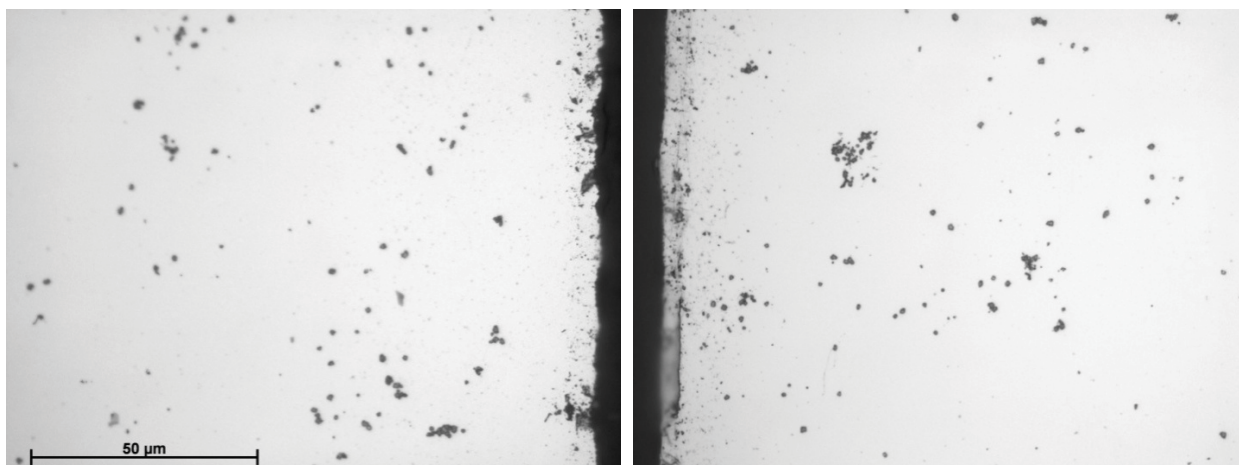


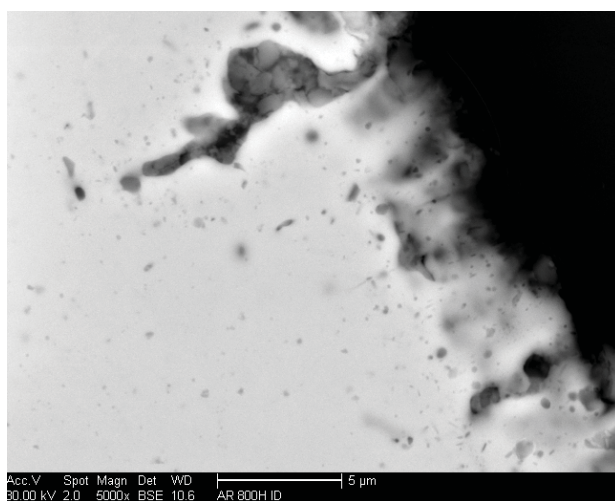
Figure 7. Configuration of the test sample.

The microstructure of the as-received tube stock was examined by SEM. In general, the tube surfaces of none of the alloys exhibited any surface oxides, and appeared to have been thoroughly descaled by the manufacturer. However, the internal and external surfaces of alloy tubes were rough from the manufacturing process, with convoluted surfaces that were a few microns deep as if from mechanical abrasion or grain boundary attack by the manufacturer's descaling process. Generally, the roughened layer was thicker at the internal surfaces of the tubes than at the external surface. In addition, small isolated pockets of internal oxide (as subsurface oxide inclusions) were evident near the surfaces; isolated fingers of internal oxide extended as much as 10 microns deep, as shown in Figure 8 for Incoloy 800H. The bulk microstructure contained numerous carbide and carbonitride precipitates throughout the samples. However, the precipitates were distributed nonhomogeneously; some areas of the samples showed almost no carbides, whereas others showed groups of coarse precipitates. The microstructure of Inconel 617 was similar, exhibiting carbide and carbonitride precipitates in the bulk of the alloy, and internal oxide inclusions in the subsurface of the tubes, generally less than 5 microns deep as shown in Figure 9. The microstructure of the Haynes 230 tube stock exhibited a high frequency of Ni-Cr-W precipitates in the grain boundaries and the matrix of the alloy, appearing as white spots in Figure 10, as well as Ni-Al-Cr precipitates, appearing as dark spots near the surface of the tube. Energy dispersive analysis showed no evidence of oxide precipitates in the subsurface of the Haynes 230, unlike the Incoloy 800H and Inconel 617.



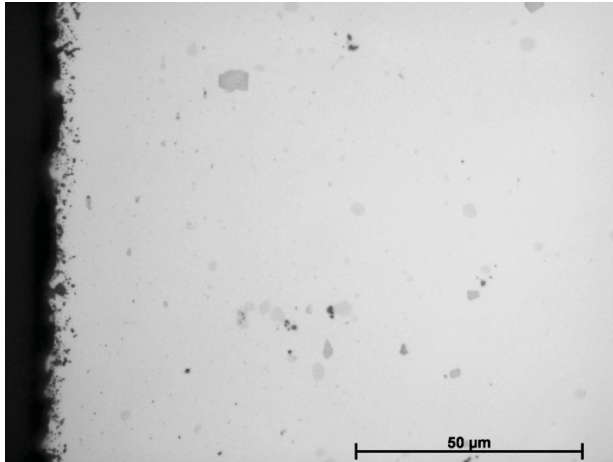
(a) Incoloy 800H, cross section at outer edge

(b) Incoloy 800H cross section at inner edge

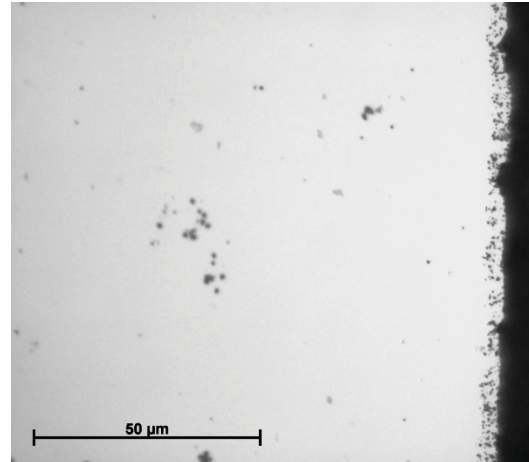


(c) Finger of internal oxide.

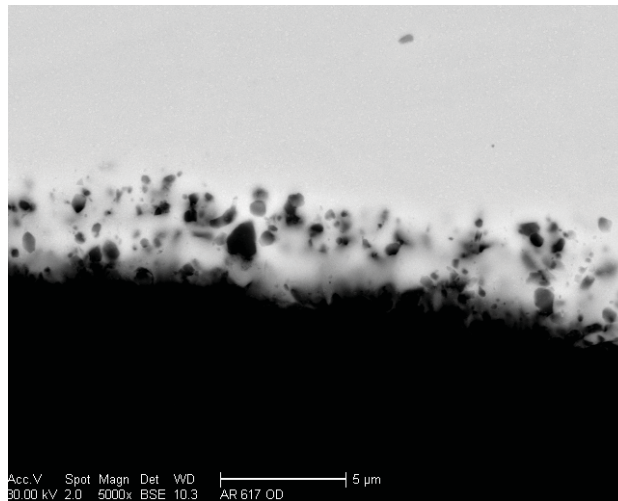
Figure 8. Microstructure of the cross section of as-received Incoloy 800H tube stock.



(a) Inconel 617 cross section at inner edge



(b) Inconel 617 cross section at outer edge



(c) Subsurface internal oxides.

Figure 9. Microstructure of the cross section of as-received Inconel 617 tube stock.

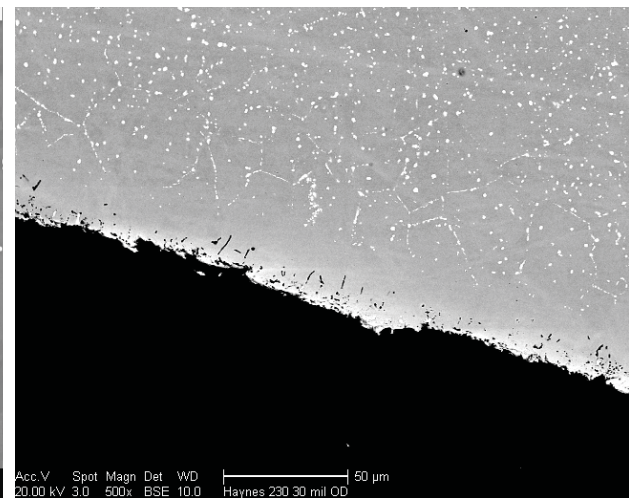
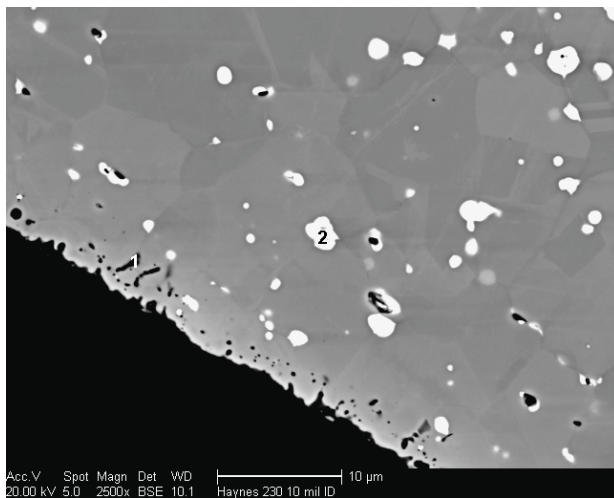


Figure 10. Microstructure of the cross section of as-received Haynes 230 tube stock.

3.3 Gas Mixtures

The probe gas used in the primary gas loop of the system for the hydrogen permeability measurements consisted of commercial mixtures of hydrogen in high-purity helium at nominal concentrations of 100, 1,000, and 10,000 ppm. The actual concentrations (100, 984, and 10,000 ppm) were certified by the vendor for each bottle of gas, and were verified in use by mass spectrometry. Ultra-high purity helium gas was used as the sweep gas in the secondary gas loop of the system.

3.4 Test Parameters

The gas permeability of materials depends on the sample temperature, the wall thickness and heated area of the sample, and the partial pressure of hydrogen on both sides of the sample. Furthermore, permeability is affected by the condition of the metal surface and in particular by its oxidation state. The permeability is evaluated by measuring the flux of hydrogen molecules entering the secondary loop. This in turn is derived by measuring the total volumetric helium flow rate in the secondary loop and the concentration of hydrogen in the helium flow. The following are therefore the parameters that were measured or otherwise controlled during the tests:

- Sample temperature and heated area, including the temperature distribution over the active heated area of the sample
- Concentration of hydrogen in the primary and secondary loops
- Flow rate of helium in secondary loop input line
- Total pressure in primary and secondary loops
- Sample composition, wall thickness, and surface condition.

With the exception of sample composition and surface condition, these parameters are used directly in the data reduction to determine the permeability of the material.

To simplify the control of sweep gas composition and data analysis, the permeability measurements were performed in the single-pass mode of operation for hydrogen tests rather than recirculation mode. In the single-pass mode, the helium sweep gas in the secondary loop was exhausted from the system after being sampled to measure composition, rather than being recirculated through the loop. The permeability was measured with hydrogen-helium probe gas mixtures containing nominally 100, 1,000, and 10,000 ppm hydrogen in helium at a total pressure of 0.9 to 0.95 atm. The measurements were made at sample temperatures in the range of 650 to 950°C (usually at increments of 50 to 100°C). Because the thinner wall resulted in shorter equilibration times, the tests at 650 to 850°C were usually conducted on samples with 0.010 in. (0.254 mm) wall thickness. For Inconel 617, coupling of the induction heater power to the 0.010 in. (2.54 mm) samples was insufficient to heat the 0.010-in.-thick samples above 900°C. Therefore, measurements at 900 and 950°C for that alloy were conducted on samples with 0.030 in. (0.762 mm) wall thickness for better coupling.

3.5 Reference Materials

The NGNP objective of the permeability determination activity is to ultimately measure the permeability of tritium through the alloys that are candidates for NGNP structural components. The technical approach for the activity was to test and validate the operation of the permeability measurement system using hydrogen and a reference alloy with known permeation characteristics, and then to determine the hydrogen permeability for the candidate alloys before proceeding with the tritium measurements. Using this approach, problems with system performance can be resolved during the

hydrogen testing phase, when special handling procedures for radiation contamination control are not required.

As indicated by Figure 2 and Table 1, there are nine published reports for the permeability of hydrogen through Incoloy 800/800H, with fairly consistent grouping of the data. The elemental composition specifications for Incoloy 800 and 800H are identical, the difference being solution heat treatment and better carbon control for Incoloy 800H.^{11,14,15,16} Incoloy 800H was more readily available in tube stock than Incoloy 800. Therefore, even though more permeation data were available for Incoloy 800, Incoloy 800H was chosen as the reference material for validating the performance of the measurement system during the hydrogen tests.

4. MEASUREMENT RESULTS

The hydrogen permeability tests used Incoloy 800H as reference material for testing the performance of the permeability measurement system, hydrogen as the permeating gas, and single-pass mode of operation. The alloys Inconel 617 and Haynes 230 were tested similarly. In this mode of operation, the partial pressure of hydrogen in the primary loop was constant, and the hydrogen flux entering the secondary loop increased sigmoidally until equilibrium concentration was reached, as measured by the in-line Inficon mass spectrometer. An example of the hydrogen concentration equilibration in the secondary loop in a permeation test is given in Figure 11 for Incoloy 800H tested at 800°C with 10,000 ppm hydrogen-helium in the primary loop.

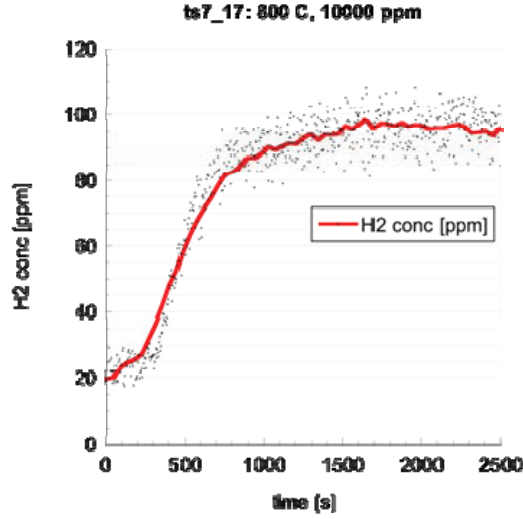


Figure 11. Example of hydrogen flux through a sample in a test, as measured by the rise in hydrogen concentration in the sweep gas flow of the secondary loop.

Hydrogen permeation through most metals is governed by the permeation model^{4,5, 10,11,17,18,}

$$J_{H_2} = \frac{K_{H_2}}{x} (\sqrt{P_{H_2}^1} - \sqrt{P_{H_2}^2}) \quad (1)$$

where: J_{H_2} is the hydrogen flux through the sample, K_{H_2} is the hydrogen permeability of the sample, x is the thickness of the sample, $P_{H_2}^1$ is the input pressure of hydrogen permeation gas on the inlet (high pressure) side of the sample, and $P_{H_2}^2$ is the output pressure of permeated hydrogen. The hydrogen flux through the sample, J_{H_2} , is equal to the area-normalized volumetric flow rate of the permeated hydrogen, \dot{V}_{H_2} , and can be expressed in terms of the concentration of permeated hydrogen, C_{H_2} , in the helium sweep flow, \dot{V}_{He} , of the secondary loop, and the heated area, A , of the sample

$$J_{H_2} = \frac{C_{H_2} \dot{V}_{He}}{A} \quad (2)$$

Therefore, by combining Equations 1 and 2, the temperature-specific permeability coefficient, $K_{H_2}^T$, can be expressed in terms of the concentration of permeated hydrogen, C_{H_2} , in the helium sweep flow,

\dot{V}_{He} , of the secondary loop, the heated area, A , of the sample, and the partial pressures of input hydrogen, $P_{H_2}^1$, and permeated hydrogen, $P_{H_2}^2$.

$$K_{H_2}^T = \frac{C_{H_2} \cdot \dot{V}_{He} \cdot x}{A \cdot (\sqrt{P_{H_2}^1} - \sqrt{P_{H_2}^2})} \quad (3)$$

When the value of $P_{H_2}^2$ is negligible, the expression for $K_{H_2}^T$ simplifies to

$$K_{H_2}^T = \frac{C_{H_2} \cdot \dot{V}_{He} \cdot x}{A \cdot \sqrt{P_{H_2}^1}} \quad (4)$$

The temperature dependence of permeability coefficient, $K_{H_2}^T$, is given by the Arrhenius expression

$$K_{H_2}^T = K_0 \exp^{-Q/RT} \quad (5)$$

where: K_0 is the temperature-independent permeability constant, Q is the activation energy of permeation, R is the universal gas constant, and T is absolute temperature. Therefore, for K_0 and Q for a permeation system, one can calculate the temperature-specific permeability, $K_{H_2}^T$, for any absolute temperature, T , within the temperature range for which the source data are valid.

The hydrogen flux through the test samples, and the hydrogen permeability, were calculated from the following data directly measured in the permeation tests:

- Total gas pressure in the primary loop, P_{tot}^1
- Concentration of hydrogen in the helium of the primary loop, $C_{H_2}^1$ (controlled by use of vendor-certified gas mixtures and confirmed by in-line gas analysis)
- Total gas pressure in the secondary loop, P_{tot}^2
- Flow rate of helium in the secondary loop, \dot{V}_{He}
- Gross concentration of hydrogen after permeation equilibrium was achieved in secondary loop, C_{tot}^2
- Average sample temperature
- Heated length, L , of the sample.

The wall thickness, x , of the samples was measured off-line by destructive methods (described earlier). In addition, the background hydrogen concentration in the secondary loop system, C_{bg} , was determined in blank runs after the permeation tests. The data collected in the permeability tests of the three alloys are summarized in Tables A-1, B-1, and C-1 of Appendices A, B, and C. The hydrogen permeation flux and the permeability were calculated from the raw data using the following relationships. The hydrogen permeation flow rate through the wall of the sample, \dot{V}_{H_2} (in units of $\text{cm}^3(\text{STP})/\text{sec}$), was calculated from the helium flow rate in the secondary loop, \dot{V}_{He} , and the hydrogen concentration in the secondary loop at permeation equilibrium, C_{tot} , corrected for the hydrogen system background concentration, C_{bg} , with conversion from concentration units of ppm to volume fraction as

$$\dot{V}_{H_2} = \dot{V}_{He} \cdot (C_{tot} - C_{bg}) \cdot 10^{-6}. \quad (6)$$

The inlet hydrogen pressure in the primary loop, $P_{H_2}^1$ (atm), was calculated from the total gas pressure in the primary loop, P_{tot}^1 (in units of Pa), and the hydrogen concentration in the input gas in the primary loop, $C_{H_2}^1$ (in units of ppm), with conversion factors to convert pressure and concentration units from Pa and ppm to atmospheres as

$$P_{H_2}^1 (\text{atm}) = P_{tot}^1 (\text{Pa}) \cdot C_{H_2}^1 \cdot (10^{-6}/101325 \text{ Pa/atm}). \quad (7)$$

Similarly, the outlet hydrogen pressure, which is the partial pressure of permeated hydrogen in the helium sweep flow of the secondary loop, $P_{H_2}^2$, was calculated from the total gas pressure in the secondary loop, P_{tot}^2 , and the measured hydrogen concentration in the helium sweep flow, C_{tot}^2 corrected for the hydrogen background in the secondary loop, C_{bg}^2 :

$$P_{H_2}^2 = P_{tot}^2 \cdot (C_{tot}^2 - C_{bg}^2) \cdot (10^{-6}/101325 \text{ Pa/atm}). \quad (8)$$

The flux of permeated hydrogen, J_{H_2} (in units of $\text{cm}^3 \text{ (STP)}/\text{cm}\cdot\text{s}\cdot\text{atm}^{1/2}$), across the sample wall was calculated from the hydrogen permeation flow rate, \dot{V}_{H_2} , normalized for the heated surface area (tube circumference and heated length, L) by Equation 2 above, and more explicitly by

$$J_{H_2} = \dot{V}_{H_2} / (\pi \cdot D \cdot L). \quad (9)$$

The permeability was calculated from the hydrogen flux, J_{H_2} , wall thickness of the sample, x , and the inlet and outlet partial pressures of hydrogen using Equations 3 and 4. The data were reduced with both Equations 3 and 4 because of the inability to measure the rise of the background system hydrogen directly during the course of the tests. Therefore, Equation 4 may represent the initial stages of each test, where the background hydrogen pressure is negligible, and Equation 3 the test at final equilibrium, where the background hydrogen pressure has risen to significant values. Equation 3, which adjusts the permeability for the system hydrogen background, results in higher permeation rates and permeability values (the upper bound for permeability), while Equation 4 results in lower values (lower bound). Because of the uncertainty in the partial pressure of background system hydrogen during the course of the tests, both values were summarized for each test as the upper and lower permeability limits in Tables A-2, B-2, and C-2 in the appendices. For simplicity, an arithmetic average of the two permeability values was generated and reported as such in Tables A-2, B-2, and C-2 and is used to summarize the results.

Finally, the permeation activation energy, Q , and the temperature-independent permeation constant, K_0 , were generated by regression fits to the reduced data using Equation 5. The results for the three alloys are summarized in Table 5. In principle, because the permeability expression normalizes the permeation flux for driving pressure as indicated by Equation 3, each of the three gas mixtures used in the tests of each alloy should have produced the same permeability-temperature correlations. However, for all three alloys, the 100 ppm hydrogen-helium mixture produced somewhat higher permeability values than the 1,000 ppm and 1% hydrogen-helium mixtures. The apparent higher permeability from the 100 ppm hydrogen tests may have at least two possible causes: a sample ‘memory’ effect, in which dissolved hydrogen may outgas from the sample; and outgassing of adsorbed hydrogen from the system surfaces during the course of the test. At the low driving pressure of 100 ppm hydrogen, at which the hydrogen flux through the sample will be low, either effect could contribute spuriously but significantly to the measured hydrogen flux and hydrogen concentration in the secondary loop, thereby overstating the permeability. The cause of the deviation has not been established, but will be evaluated in further tests with very low partial pressures of tritium. Therefore, the 100 ppm hydrogen data sets were not used to generate the data in Table 5.

Table 5. Measured hydrogen permeability values of Incoloy 800H, Inconel 617, and Haynes 230.

Alloy	K_0 $\text{cm}^3 \text{ (STP)}/\text{cm}\cdot\text{s}\cdot\text{atm}^{1/2}$	Q kcal/mol	
Incoloy 800H	0.359	21.6	Average value
	0.816	23.0	Upper limit
	0.120	19.6	Lower limit
Inconel 617	0.539	21.3	Average value
	0.815	22.0	Upper limit

	0.326	20.5	Lower limit
Haynes 230	0.534	22.0	Average value
	0.884	22.9	Upper limit
	0.287	20.9	Lower limit

In addition, the 1% hydrogen data set for Incoloy 800H was flawed because of slight oxidation of Incoloy 800H and consequently slight suppression of the permeation rate, despite the use of high purity gases. Unfortunately, the 1% hydrogen tests were the final tests with the particular Incoloy 800H sample before it was retired, and the effects of oxidation became measureable in that final series of tests. In that series of tests, temperatures below 900°C caused slight surface oxidation of the alloy and measurably depressed the permeation rate. This effect was not observed during the course of the tests with Inconel 617 and Haynes 230. These observations of sensitivity of Incoloy 800/800H towards oxidation (even in high purity gases) and the suppression of permeability by the resultant surface oxide are consistent with literature reports.^{2,4,11,13,14,17} The permeability suppression factor by oxides grown in situ from impurities in the sweep gas have been reported to be about 100 for Inconel 617 and as high as 3,000 for Incoloy 800/800H.^{11,19} Growth of oxide is sensitive to the impurity levels in the hydrogen or helium, the hydrogen pressure, and temperature.^{11,14}

Because the intermediate data for the 1% hydrogen tests were suspect, that data set was also excluded for Incoloy 800H. Therefore, the permeation activation energy and permeability constant for Incoloy 800H were determined only with the 1,000 ppm hydrogen data set. The 1% hydrogen data set will be repeated at a later date.

As shown in Table 6, the Incoloy 800H permeability data from this work compare well with published literature values for Incoloy 800 and 800H. (The two alloys have the same elemental composition specifications and differ only in heat treatment, so that permeability is expected to be the same for both alloys.) The present data compares well with the historical data, even though the present data were obtained at significantly lower partial pressures of hydrogen than the historical data. The comparison with literature data is shown graphically in Figure 12, and illustrates the scatter in the historical data. In that context, the permeability data obtained from this work compare well, even though they are at the low end of the published range of values, and also exhibit a slightly higher activation energy and therefore slightly higher temperature dependence.

Table 6. Comparison of measured hydrogen permeability of Incoloy 800H with literature values for Incoloy 800/800H.

K_0 $\text{cm}^3 \text{H}_2 \text{ (STP)/cm}\cdot\text{sec}\cdot\text{atm}^{1/2}$	Q kcal/mol	Temp. Range °C	Pressure Range atm	References
Incoloy 800/800H				
3.59×10^{-1} (1)	21.6 (1)	650–950	0.001–0.01	This work
5.90×10^{-2} (1)	15.5 (1)	450–950	5–10	9,11
9.24×10^{-2} (1)	18.0 (1)	750–950	<40	5
7.39×10^{-2}	17.7	600–950	5×10^{-4} – 0.5	4
1.76×10^{-2}	15.3	700–950	1–5	2
7.58×10^{-2}	16.8	760–960	1	8
4.03×10^{-1}	20.6	600–1050	1–10	7
4.02×10^{-2}	15.5	450–950	5–10	9,11
6.02×10^{-2}	16.6	500–1000	0.1–1	3

2.44×10^{-3}	13.1	300–600	0.13–0.8	6
Inconel 617				
5.39×10^{-1}	21.3	650–950	0.001–0.01	This work
2.28×10^{-1}	18.9	600–1050	1–10	7
1.39×10^{-1}	19.8	750–950	<40	5
* Data for Incoloy 800H.				

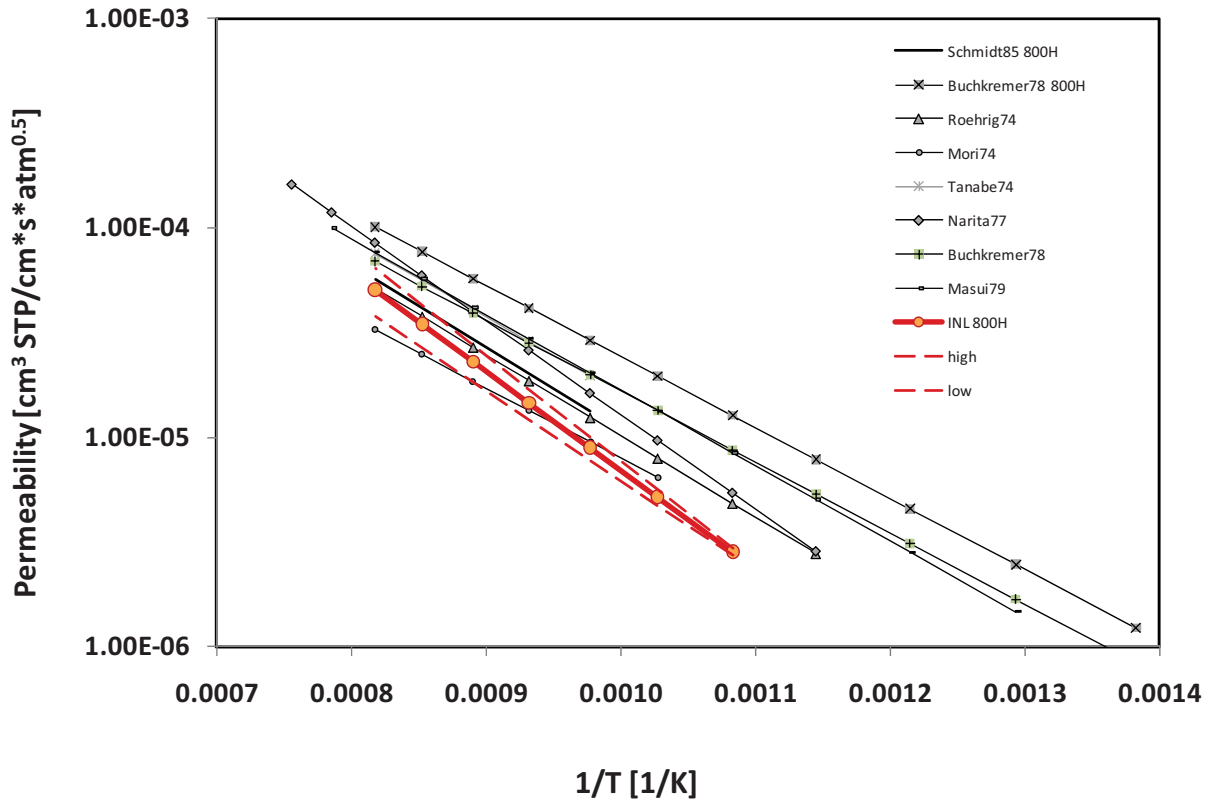


Figure 12. Hydrogen permeability of Incoloy 800H from this work compared with published data, and show the uncertainty limits of the data.

Similarly, the hydrogen permeability data for Inconel 617 are compared with the two known sets of published values in Table 6 and Figure 13. Inconel 617 permeability data from this work compare very well with the data of Narita⁷ and of Schmidt et al.,⁵ even though the driving hydrogen pressures are several orders of magnitude lower than those used by Narita or by Schmidt et al. As with the Incoloy 800H data, the figure shows the average Inconel 617 permeability along with upper and lower limits for the data set. The data from this work shows a slightly steeper slope (somewhat higher activation energy) than the data of Schmidt et al. and of Narita, and therefore a slightly greater temperature dependence of the permeability coefficient.

The Haynes 230 data are plotted in Figure 14 in similar manner. The Haynes 230 data are compared only with the Incoloy 800H data from this work, because published permeability data for this alloy have not been found in the open literature. The Haynes 230 has slightly higher permeability than the Incoloy 800H. However, the slope of the Haynes 230 data is comparable to that of Incoloy 800H, indicative of comparable temperature dependence of the permeability.

As indicated in Table 3, Inconel 617 and Haynes 230 have similar nickel composition, with 53.0 and 59.5 wt% nickel, respectively, and less than 1.6 wt% iron. In comparison, Incoloy 800H has significantly lower nickel and higher iron content, 30.8 and 46.6 wt%, respectively. As summarized in Table 5, the results of this work show that the permeability of Inconel 617 and Haynes 230 is comparable, with similar permeation constant and activation energy. While the permeation activation energies of the three alloys are similar, the permeation constants for Inconel 617 and Haynes 230 are about 50% greater than the permeation constant for Incoloy 800H. These results are consistent with the observation that hydrogen permeability of alloys generally increases with increasing nickel content, although the correlation is not a sensitive one.^{3,14}

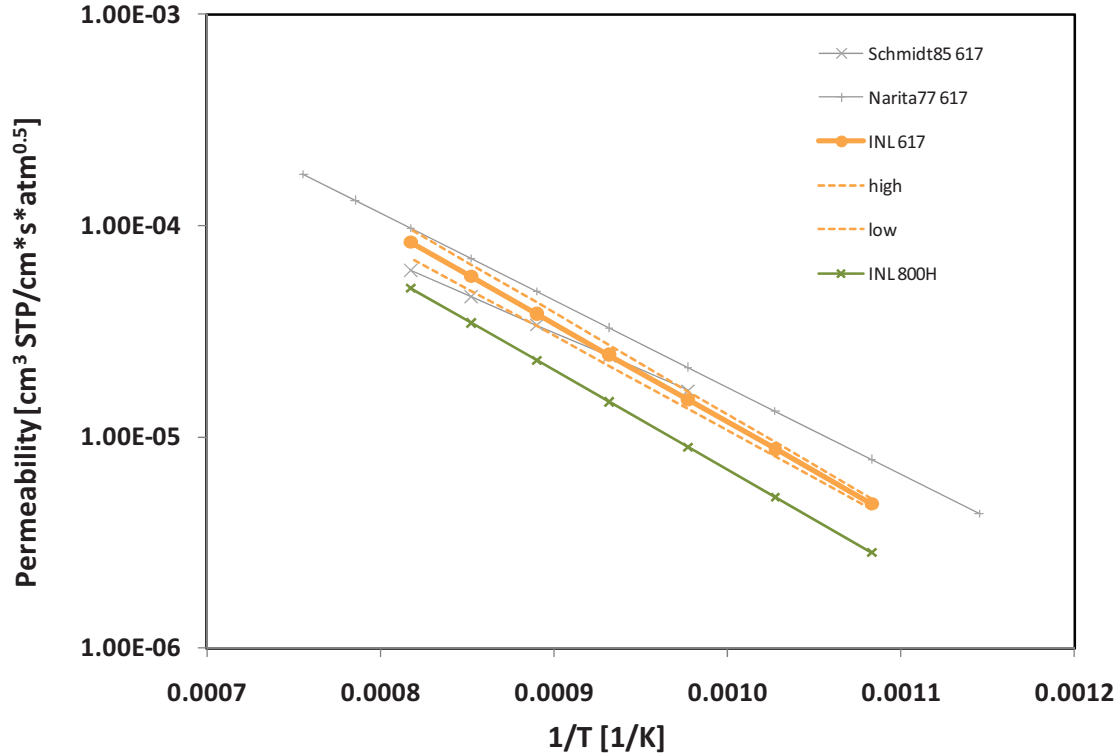


Figure 13. Hydrogen permeability of Inconel 617 compared with the Incoloy 800H data from this work and the two sets of published data.

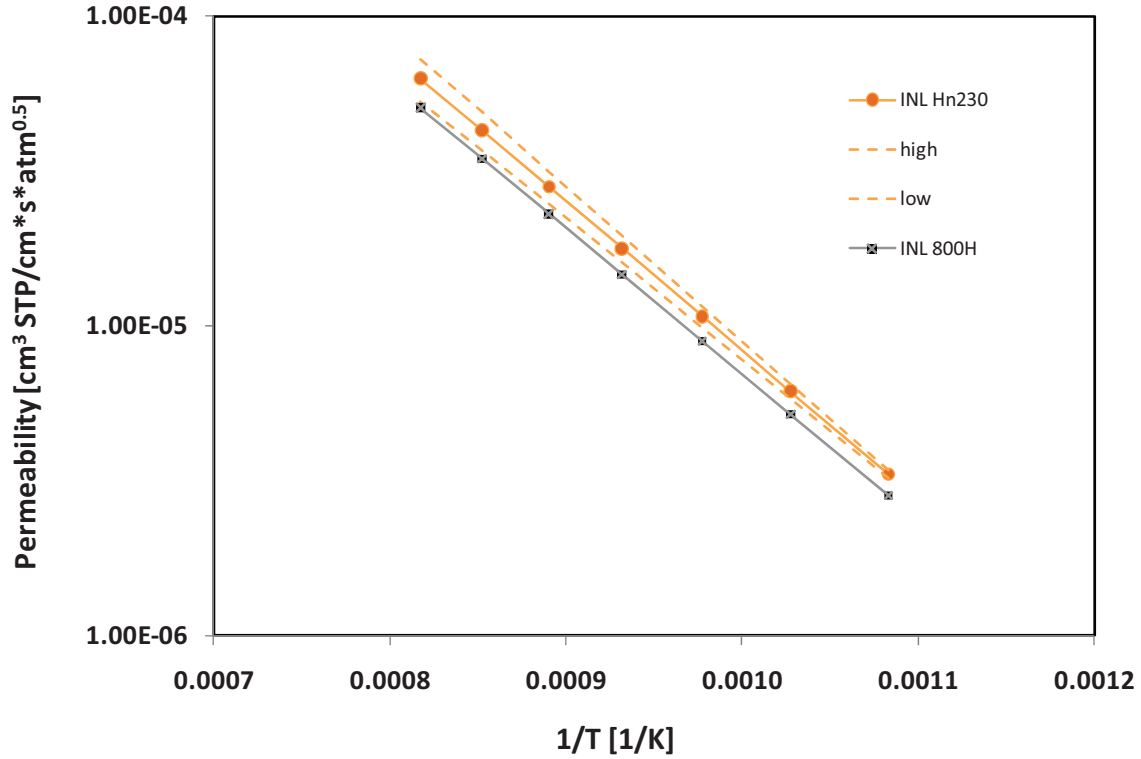


Figure 14. Hydrogen permeability of Haynes 230 compared with the Incoloy 800H data from this work.

5. CONCLUSIONS

A potential issue in the design of the NGNP reactor and high-temperature components is the permeation of fission generated tritium and product hydrogen through the high-temperature components such as the heat exchanger. Such permeation can result in the loss of fission-generated tritium to the environment and the potential contamination of the helium coolant by permeation of product hydrogen into the coolant system. The issue will be addressed in the engineering design phase, and requires knowledge of permeation characteristics of the candidate alloys. Of three potential candidate alloys for high-temperature components of the NGNP reactor design, the hydrogen permeability has been documented well for only Incoloy 800H. Hydrogen permeability data have been published for Inconel 617, but only in two literature reports and for partial pressures of hydrogen greater than one atmosphere, far higher than anticipated in the NGNP reactor. The hydrogen permeability of Haynes 230 has not been published. To support engineering design, the hydrogen permeability of Haynes 230 needed to be determined, and the published permeability of Inconel 617 needed to be validated.

A system was designed, fabricated, and tested for measuring the permeability of metal alloys at high temperatures. The system uses counter-flow gas loops with calibrated mass flow and pressure controllers, an induction heater to heat the tubular sample to temperatures in the range 650 to 950°C, a mass spectrometer for measuring the hydrogen concentrations in the gas loops, an internal calibrated thermocouple for controlling the sample temperature, and an infrared thermal imaging system for measuring the temperature distribution in the heated sample. The operation of the system was tested and validated using Inconel 800H, for which hydrogen permeation data have been published in several journal articles. Using this system, the temperature-independent permeability constant and permeation activation energy were found to be 0.359 cm³ hydrogen (STP)/cm²·sec·atm^{1/2} and 21.6 kcal/mol, respectively, comparable to the published values for this alloy.

The system was used to measure the permeability of Inconel 617 and Haynes 230 at hydrogen partial pressures of 10^{-3} and 10^{-2} atmospheres, significantly below the hydrogen pressures used in the published data for Inconel 617. The temperature-independent permeability constant and the activation energy were measured as $0.539 \text{ cm}^3 \text{ hydrogen (STP)/cm}\cdot\text{sec}\cdot\text{atm}^{1/2}$ and 21.3 kcal/mol , respectively, for Inconel 617, in good agreement with the two sets of published values obtained at hydrogen pressures at one atmosphere and greater. The temperature-independent permeability constant and the activation energy for Haynes 230 were measured as $0.534 \text{ cm}^3 \text{ hydrogen (STP)/cm}\cdot\text{sec}\cdot\text{atm}^{1/2}$ and 22.0 kcal/mol , respectively. These results indicate that hydrogen permeability of Inconel 617 and Haynes 230 is about 50% higher than for Incoloy 800H, and that temperature sensitivity is comparable.

6. REFERENCES

1. D. L. Hanson, *Test Plan for Characterizing Tritium Transport in a VHTR*, PC-000550-0, General Atomics, San Diego, CA, December 20, 2007.
2. Y. Mori, H. Ikegami, and T. Nakada, 1974, "49. High temperature helium heat exchange loop," *BNES Conference on the HTR and Process Applications, Institute of Civil Engineering, Westminster, London, November 26-28, 1974*, paper 49, pp 49.1-49.12.
3. K. Masui, H. Yoshida, and R. Watanabe, "Hydrogen Permeation through Iron, Nickel, and Heat Resisting Alloys at Elevated Temperatures," *Transactions of the Iron and Steel Institute of Japan*, Vol. 19, Issue 9, 1979, pp. 547–552.
4. H. D. Roehrig, R. Hecker, J. Blumensaat, and J. Schaefer, "50. Experimental facilities for the investigation of hydrogen and tritium permeation problems involved with steam methane reforming by nuclear process heat," *BNES Conference on the HTR and Process Applications, Institute of Civil Engineering, Westminster, London, November 26–28, 1974*, paper 49, pp 50.1-50.11. Also, H. D. Roehrig, R. Hecker, J. Blumensaat, and J. Schaefer, "Studies on the Permeation of Hydrogen and Tritium in Nuclear Process Heat Installations," *Nuclear Engineering and Design*, Vol. 34, 1975, pp. 157–167.
5. A. S. Schmidt, F. Verfuss, and E. Wicke, "Studies on the permeation of hydrogen and tritium through heat resistant alloys," *Journal of Nuclear Materials*, Vol. 131, Issues 2-3, 1985, pp. 247–260.
6. T. Tanabe, S. Imoto, and Y. Miyata, "Hydrogen Permeation through Incoloy 800," *Journal of Nuclear Science and Technology*, Vol. 16, Issue 4, 1979, pp. 310–302.
7. Y. Narita, "Study on Hydrogen Permeation through Super Alloys," *Proceedings of the Japan-U.S. Seminar on HTGR Safety Technology*, Helium Technology Volume II, BNL-NUREG-50689-Vol. II, Brookhaven National Laboratory, Upton, New York, September 15–16, 1977, pp. 71–85.
8. T. Tanabe, INTOR Study Group Report (IAEA 1979), EUR FU BRU/XII 501/79/EDV 80, 1974, cited by A. D. Le Claire, "Permeation of Gases Through Solids III-As Assessment of Measurements of the Steady State Permeability of H and its Isotopes through Ni and through Several High Ni Commercial Alloys and Steels," AERE-R-10846, United Kingdom Atomic Energy Authority Harwell, March 1983.
9. H. P. Buchkremer, H. J. Cordewiner, W. Diehl, G. Esser, D. Fischmann, R. Hecker, M. Hishida, J. Lambrecht, V. Malka, R. Raitz von Frentz, H. D. Roehrig, A. Tauber, and J. Schaefer, *Ueberblick ueber die neueren Arbeiten auf dem Gebiet des Wasserstoff- und Tritiumverhaltens in Hochtemperaturreaktoren*, Juel-1497, Kernforschungsanlage Juelich, GmbH, Contributions of the Institute of Reactor Development to the II Seminar on Hydrogen and Tritium Behavior in HTRs, March 8, 1978.
10. S. Bhattacharyya, E. J. Veserly, Jr., and V. L. Hill, *Determination of Hydrogen Permeability in Uncoated and Coated Superalloys, Interim Report*, DOE/NASA/0006-1, NASA CR-165209, prepared by Illinois Institute of Technology Research Institute, Chicago, IL, for the National Aeronautics and Space Administration, Lewis Research Center, January 1981.
11. J. Schaefer, D. Stoeber, and R. Hecker, "Terms and Results of Hydrogen Permeation Testing of Oxide-Scaled High-Temperature Alloys," *Nuclear Technology*, Vol. 66, 1984, pp. 537–549.
12. J. T. Bell, J. D. Redman, and H. F. Bittner, "Tritium Permeation through Clean Construction Alloys," *Journal of Materials for Energy Systems*, Vol. 1, 1979, pp. 55–59.

13. J. T. Bell, J. D. Redman, and H. F. Bittner, "Tritium Permeation through Clean Incoloy 800 and Sanicro 31 Alloys and through Steam Oxidized Incoloy 800," *Metallurgical Transactions A*, Vol. 11A, 1980, pp. 775–782.
14. A. D. Le Claire, *Permeation of Gases Through Solids III-As Assessment of Measurements of the Steady State Permeability of H and its Isotopes through Ni and through Several High Ni Commercial Alloys and Steels*, AERE-R-10846, United Kingdom Atomic Energy Authority Harwell, March 1983.
15. High Temp Metals, Inc., <http://www.hightempmetals.com>.
16. MegaMex, Inc., <http://www.megamex.com>.
17. R. A. Strehlow and H. C. Savage, "The Permeation of Hydrogen Isotopes through Structural Metals at Low Pressures and through Metals with Oxide Film Barriers," *Nuclear Technology*, Vol. 22, 1974, pp. 127–137.
18. W. M. Robertson, 1972, "Hydrogen Permeation, Diffusion and Solution in Pure Nickel and a Nickel Based Superalloy," *International Meeting on Hydrogen in Metals, Vol II, Kernforschungsanlage Juelich, Germany, March 20-24, 1972*, pp. 449–491.
19. H. P. Buchkremer, R. Hecker, and D. Stoeber, "Hydrogen Permeation through Passive Layers on Austenitic High Temperature Alloys," *Passivity of Metals and Semiconductors*, M. Froment, ed., Elsevier Science Publishers B. V., Amsterdam, Netherlands, 1983, pp. 675–680.

Appendix A

Summary of Incoloy 800H Permeability Data

Appendix A

Summary of Incoloy 800H Permeability Data

A total of 26 permeability measurement tests were performed with Incoloy 800H. The first 12 measurements were performed before the thermal imaging system was acquired and installed in the measurement system. The first 12 tests were conducted with a thermocouple in contact with the outer surface of the heated zone of the sample, which gave only single-point temperature measurement for the heated zone of the sample, and were performed solely to test the operation of the system. Subsequent tests with the thermal imaging system, together with a thermocouple mounted within the sample tube in contact with the inner sample surface, indicated significant errors in the readings from the externally mounted thermocouple of the first series of tests. Because of the uncertainty about the sample temperature and the average temperature over the heated area, the data of first 12 tests were not used in determining the permeability of Incoloy 800H. The individual measurement data, hydrogen flux, and permeabilities obtained from the remaining 14 tests, which were performed with the thermal imaging system and an internal reference thermocouple in place, are summarized in the tables of this appendix.

Table A-1. Test parameters and hydrogen permeation flow data for Incoloy 800H.

Test	Set Point Temp °C	Average Temp °C	Primary Loop		Secondary Loop				Sample	
			Total Pressure, P^1_{tot} , Pa	H ₂ Conc, $C^1_{H_2}$, ppm	He flow, \dot{V}_{He} , cm ³ (STP)/min	Total Pressure, P^2_{tot} , Pa	Equilib H ₂ Conc, C^2_{tot} , ppm	Backg'd H ₂ Conc., C^2_{bg} , ppm	H ₂ Permeation Flow, \dot{V}_{H_2} , cm ³ (STP)/sec	Heated Length L, cm
TS7-19	650	648	94100	10,000	100	96000	30	20	1.65E-05	2.5
TS7-18	700	698	94700	10,000	100	93800	37	17	3.32E-05	2.75
TS7-20	750	741	94500	10,000	100	94400	45	25	3.32E-05	2.75
TS7-17	800	787	95100	10,000	100	96600	72	11	1.01E-04	3.68
TS7-21	850	833	94200	10,000	100	111100	115	12	1.72E-04	3.68
TS7-16	900	883	95100	10,000	100	96600	239	11	3.81E-04	3.85
TS7-13	650	648	95000	984	100	95400	17	8	1.49E-05	2.5
TS7-8	700	698	95100	984	100	95000	34	17	2.97E-05	2.75
TS7-7	800	787	95000	984	100	94800	84	17	1.12E-04	3.68
TS7-5	900	883	95000	984	100	93500	141	6	2.24E-04	3.68
TS7-6	950	937	95000	984	100	95200	176	14	2.71E-04	3.85
TS7-12	800	787	95100	100	100	94600	35	12	3.90E-05	3.68
TS7-10	900	883	95100	100	100	95200	61	15	7.62E-05	3.85
TS7-9	950	937	95100	100	100	94100	74	12	1.04E-04	3.85

Table A-2. Hydrogen permeability coefficients for Incoloy 800H.

Test	Ave. Temp. °C	Sample Thickness x, cm	Inlet H ₂ Pressure, $P_{H_2}^1$, atm	Outlet H ₂ Pressure, $P_{H_2}^2$, atm	Hydrogen Flux J_{H_2} , cm ³ (STP)/cm ² ·s	Permeability $K_{H_2}^T$ cm ³ /cm·s·atm ^{1/2}		
						Lower limit	Upper limit	Average
TS7-19	648	0.0254	9.29E-03	9.39E-06	3.31E-06	8.73E-07	9.02E-07	8.87E-07
TS7-18	698	0.0254	9.35E-03	1.85E-05	6.06E-06	1.59E-06	1.67E-06	1.63E-06
TS7-20	741	0.0254	9.33E-03	1.85E-05	6.05E-06	1.59E-06	1.66E-06	1.63E-06
TS7-17	787	0.0254	9.39E-03	5.78E-05	1.38E-05	3.61E-06	3.92E-06	3.76E-06
TS7-21	833	0.0254	9.30E-03	1.13E-04	2.34E-05	6.16E-06	6.93E-06	6.54E-06
TS7-16	883	0.0254	9.39E-03	2.18E-04	4.96E-05	1.30E-05	1.53E-05	1.42E-05
TS7-13	648	0.0254	9.23E-04	8.41E-06	2.98E-06	2.50E-06	2.76E-06	2.63E-06
TS7-8	698	0.0254	9.24E-04	1.67E-05	5.41E-06	4.52E-06	5.22E-06	4.87E-06
TS7-7	787	0.0254	9.23E-04	6.30E-05	1.53E-05	1.28E-05	1.73E-05	1.50E-05
TS7-5	883	0.0254	9.23E-04	1.24E-04	3.05E-05	2.55E-05	4.03E-05	3.29E-05
TS7-6	937	0.0254	9.23E-04	1.53E-04	3.52E-05	2.95E-05	4.97E-05	3.96E-05
TS7-12	787	0.0254	9.39E-05	2.18E-05	5.31E-06	1.39E-05	2.69E-05	2.04E-05
TS7-10	883	0.0254	9.39E-05	4.30E-05	9.93E-06	2.60E-05	8.05E-05	5.33E-05
TS7-9	937	0.0254	9.39E-05	5.79E-05	1.35E-05	3.55E-05	1.65E-04	1.00E-04

Appendix B

Summary of Inconel 617 Permeability Data

Appendix B

Summary of Inconel 617 Permeability Data

Table B-1. Test parameters and hydrogen permeation flow data for Inconel 617.

			Primary Loop		Secondary Loop				Sample	
Test	Set Point Temp. °C	Average Temp. °C	Total Pressure, P^1_{tot} Pa	H ₂ Conc, $C^1_{H_2}$, ppm	He flow \dot{V}_{He} cm ³ (STP)/min	Total Pressure, P^2_{tot} Pa	Equilib H ₂ Conc, C^2_{tot} , ppm	Backg'd H ₂ Conc., C^2_{bg} , ppm	H ₂ Permeation Flow, \dot{V}_{H_2} , cm ³ (STP)/sec	Heated Length, L, cm
TS5-7	650	648	94700	10,000	200	94700	40.4	20.1	6.77E-05	2.5
TS5-5	800	787	94700	10,000	200	94200	148.8	18.6	4.34E-04	3.68
TS5-6	900	883	94600	10,000	200	94600	306.6	20	9.55E-04	3.85
TS10-5	950	937	94900	10,000	200	94400	198.8	19.2	5.99E-04	3.85
TS5-4	650	648	94900	984	200	95300	24.3	14.4	3.30E-05	2.5
TS5-1	800	787	94700	984	200	98100	79	15	2.13E-04	3.68
TS5-3a	800	787	94700	984	200	93500	71	19	1.73E-04	3.68
TS5-3b	800	787	94600	984	150	93400	86	19	1.68E-04	3.68
TS5-2	900	883	94500	984	200	95200	153	15	4.60E-04	3.85
TS10-4	950	937	94900	984	200	94800	84	16.1	2.26E-04	3.85
TS5-9a	700	698	95000	100	100	91400	24.6	13.7	1.82E-05	2.75
TS5-9b	700	698	95000	100	50	91400	34.8	13.7	1.76E-05	2.75
TS5-8a	800	787	94800	100	200	90600	29.4	13.7	5.23E-05	3.68
TS5-8b	800	787	94800	100	100	90600	48.1	13.7	5.73E-05	3.68
TS10-1	950	937	94600	100	100	96400	71	13.2	9.63E-05	3.85
TS10-2	950	937	94400	100	200	95800	62	15	1.57E-04	3.85

Table B-2. Hydrogen permeability coefficients for Inconel 617.

Test	Ave. Temp., °C	Sample Thickness, x, cm	Inlet H ₂ Pressure, $P_{H_2}^1$, atm	Outlet H ₂ Pressure, $P_{H_2}^2$, atm	Hydrogen Flux J_{H_2} cm ³ (STP)/cm ² ·s	Permeability $K_{H_2}^T$ cm ³ /cm·s·atm ^{1/2}		
						Lower limit	Upper limit	Average
TS5-7	648	0.0254	9.35E-03	1.90E-05	1.36E-05	3.56E-06	3.73E-06	3.65E-06
TS5-5	787	0.0254	9.35E-03	1.21E-04	5.91E-05	1.55E-05	1.75E-05	1.65E-05
TS5-6	883	0.0254	9.34E-03	2.68E-04	1.24E-04	3.27E-05	3.94E-05	3.60E-05
TS10-5	937	0.0762	9.37E-03	1.67E-04	7.79E-05	6.14E-05	7.08E-05	6.61E-05
TS5-4	648	0.0254	9.22E-04	9.31E-06	6.62E-06	5.54E-06	6.15E-06	5.85E-06
TS5-1	787	0.0254	9.20E-04	6.20E-05	2.91E-05	2.43E-05	3.29E-05	2.86E-05
TS5-3a	787	0.0254	9.20E-04	4.80E-05	2.36E-05	1.98E-05	2.56E-05	2.27E-05
TS5-3b	787	0.0254	9.19E-04	6.18E-05	2.28E-05	1.91E-05	2.58E-05	2.25E-05
TS5-2	883	0.0254	9.18E-04	1.30E-04	5.99E-05	5.02E-05	8.05E-05	6.53E-05
TS10-4	937	0.0762	9.22E-04	6.35E-05	2.95E-05	7.40E-05	1.00E-04	8.71E-05
TS5-9a	698	0.0254	9.38E-05	9.83E-06	3.31E-06	8.69E-06	1.28E-05	1.08E-05
TS5-9b	698	0.0254	9.38E-05	1.90E-05	3.21E-06	8.41E-06	1.53E-05	1.19E-05
TS5-8a	787	0.0254	9.36E-05	1.40E-05	7.13E-06	1.87E-05	3.06E-05	2.46E-05
TS5-8b	787	0.0254	9.36E-05	3.08E-05	7.81E-06	2.05E-05	4.81E-05	3.43E-05
TS10-1	937	0.0762	9.34E-05	5.50E-05	1.25E-05	9.89E-05	4.25E-04	2.62E-04
TS10-2	937	0.0762	9.32E-05	4.44E-05	2.04E-05	1.61E-04	5.21E-04	3.41E-04

Appendix C

Summary of Haynes 230 Permeability Data

Appendix C

Summary of Haynes 230 Permeability Data

Table C-1. Test parameters and hydrogen permeation flow data for Haynes 230.

			Primary Loop		Secondary Loop				Sample	
Test	Set Point Temp. °C	Average Temp. °C	Total Pressure, P^1_{tot} Pa	H ₂ Conc, C^1_{H2} ppm	He flow \dot{V}_{He} cm ³ (STP)/min	Total Pressure, P^2_{tot} Pa	Equilib H ₂ Conc, C^2_{tot} ppm	Backg'd H ₂ Conc. C^2_{bg} ppm	H ₂ Permeation Flow, \dot{V}_{H2} cm ³ (STP)/sec	Heated Length L, cm
TS13-7	650	648	94900	10,000	100	95100	41	22	3.17E-05	2.5
TS13-6	800	787	94400	10,000	200	94200	146	21	4.17E-04	3.68
TS13-5	850	833	94600	10,000	200	94400	215	20	6.50E-04	3.68
TS13-4	900	883	94300	10,000	200	94200	306	18	9.60E-04	3.85
TS13-9	950	937	94700	10,000	200	94900	387	22	1.22E-03	3.85
TS15-5	650	648	94700	984	200	94700	24.5	13.3	3.73E-05	2.5
TS15-6	800	787	94800	984	200	94800	44.1	16.8	9.10E-05	3.68
TS13-2	900	883	94500	984	200	94200	121	6.6	3.81E-04	3.85
TS15-7	950	937	94800	984	200	95100	147	15.9	4.37E-04	3.85
TS13-3	900	883	94300	100	200	95100	54	16	1.25E-04	3.85
TS15-2	650	648	94900	100	100	95100	50.1	10.5	6.60E-05	2.5
TS15-3	800	787	94800	100	100	94800	89.2	16.9	1.21E-04	3.68
TS15-4	950	937	94800	100	200	96800	100	12.1	2.93E-04	3.85

Table C-2. Permeability coefficients for Haynes 230.

Test	Ave. Temp. °C	Sample Thickness x, cm	Inlet H ₂ Pressure $P_{H_2}^1$ atm	Outlet H ₂ Pressure $P_{H_2}^2$ atm	Hydrogen Flux J_{H_2} cm ³ (STP)/cm ² ·s	Permeability, $K_{H_2}^T$ cm ³ /cm·s·atm ^{1/2}		
						Lower limit	Upper limit	Average
TS13-7	648	0.0254	9.37E-03	1.78E-05	6.35E-06	1.67E-06	1.74E-06	1.70E-06
TS13-6	787	0.0254	9.32E-03	1.16E-04	5.68E-05	1.49E-05	1.68E-05	1.59E-05
TS13-5	833	0.0254	9.34E-03	1.82E-04	8.85E-05	2.33E-05	2.70E-05	2.52E-05
TS13-4	883	0.0254	9.31E-03	2.68E-04	1.25E-04	3.29E-05	3.96E-05	3.63E-05
TS13-9	937	0.0254	9.35E-03	3.42E-04	1.58E-04	4.16E-05	5.15E-05	4.65E-05
TS15-5	648	0.0254	9.20E-04	1.05E-05	7.49E-06	6.27E-06	7.02E-06	6.64E-06
TS15-6	787	0.0254	9.21E-04	2.55E-05	1.24E-05	1.04E-05	1.25E-05	1.14E-05
TS13-2	883	0.0254	9.18E-04	1.06E-04	4.97E-05	4.16E-05	6.31E-05	5.24E-05
TS15-7	937	0.0254	9.21E-04	1.23E-04	5.69E-05	4.76E-05	7.51E-05	6.14E-05
TS13-3	883	0.0254	9.31E-05	3.57E-05	1.65E-05	4.34E-05	1.14E-04	7.87E-05
TS15-2	648	0.0254	9.37E-05	3.72E-05	1.32E-05	3.47E-05	9.39E-05	6.43E-05
TS15-3	787	0.0254	9.36E-05	6.76E-05	1.64E-05	4.31E-05	2.88E-04	1.66E-04
TS15-4	937	0.0254	9.36E-05	8.40E-05	3.81E-05	1.00E-04	1.90E-03	1.00E-03